Deciphering the Regulatory Logic of an Ancient, Ultraconserved Nuclear Receptor Enhancer Module

Pia D. Bagamasbad, Ronald M. Bonett, Laurent Sachs, Nicolas Buisine, Samhitha Raj, Joseph R. Knoedler, Yasuhiro Kyono, Yijun Ruan, Xiaoan Ruan, and Robert J. Denver

Department of Molecular, Cellular and Developmental Biology (P.D.B., S.R., R.J.D.), University of Michigan, Ann Arbor, Michigan 48109; Department of Biological Science (R.M.B.), The University of Tulsa, Tulsa, Oklahoma 74104; Unité Mixte de Recherche 7221 (L.S., N.B.), Muséum National d'Histoire Naturelle, Centre Nationale de Recherche Scientifique, CP32 Paris, France; Neuroscience Graduate Program (J.R.K., Y.K., R.J.D.), The University of Michigan, Ann Arbor, Michigan 48109; Genome Institute of Singapore (Y.R., X.R.), 138672 Singapore; The Jackson Laboratory of Genomic Medicine (Y.R., X.R.), Farmington, Connecticut 06030; and Department of Genetics and Developmental Biology (Y.R., X.R.), University of Connecticut, Storrs, Connecticut 06269

Cooperative, synergistic gene regulation by nuclear hormone receptors can increase sensitivity and amplify cellular responses to hormones. We investigated thyroid hormone (TH) and glucocorticoid (GC) synergy on the Krüppel-like factor 9 (*Klf9*) gene, which codes for a zinc finger transcription factor involved in development and homeostasis of diverse tissues. We identified regions of the *Xenopus* and mouse *Klf9* genes 5–6 kb upstream of the transcription start sites that supported synergistic transactivation by TH plus GC. Within these regions, we found an orthologous sequence of approximately 180 bp that is highly conserved among tetrapods, but absent in other chordates, and possesses chromatin marks characteristic of an enhancer element. The *Xenopus* and mouse approximately 180-bp DNA element conferred synergistic transactivation by hormones in transient transfection assays, so we designate this the *Klf9* synergy module (KSM). We identified binding sites within the mouse KSM for TH receptor, GC receptor, and nuclear factor κB. TH strongly increased recruitment of liganded GC receptor and serine 5 phosphorylated (initiating) RNA polymerase II to chromatin at the KSM, suggesting a mechanism for transcriptional synergy. The KSM is transcribed to generate long noncoding RNAs, which are also synergistically induced by combined hormone treatment, and the KSM interacts with the *Klf9* promoter and a far upstream region through chromosomal looping. Our findings support that the KSM plays a central role in hormone regulation of vertebrate *Klf9* genes, it evolved in the tetrapod lineage, and has been maintained by strong stabilizing selection. **(*Molecular Endocrinology* 29: 856–872, 2015)**

Thyroid hormone (TH) and corticosteroids (primarily glucocorticoids [GCs]) cooperate during organogenesis and can act synergistically to control tissue formation and remodeling. In amphibians, GC accelerates TH-dependent tadpole metamorphosis, in part by increasing tissue sensitivity to the TH signal (1, 2). In mammals, TH and GC have been shown to act synergistically to promote lung (3–5), intestinal (6), and possibly also fetal neurological development (7–10). In this way, environmental signals may be transduced into endocrine responses that enable animals to modulate developmental timing and phenotypic expression (1). However, the cellular and molecular mechanisms for hormone synergy are poorly understood.

ISSN Print 0888-8809 ISSN Online 1944-9917
Printed in USA

Received November 4, 2014. Accepted April 7, 2015.
First Published Online April 13, 2015

Abbreviations: acH3, acetylated H3; BW, body weight; 3C, chromosomal conformation capture; ChIA-PET, chromosome interaction analysis by paired end tag sequencing; ChIP, chromatin immunoprecipitation; CHX, cycloheximide; CORT, corticosterone; DMSO, dimethylsulfoxide; DNAse I, deoxyribonuclease I; dnTR, dominant negative TR; DR+4, direct repeat with 4-base spacer; eRNA, enhancer RNA; EtOH, ethanol; FBS, fetal bovine serum; GC, glucocorticoid; GR, GC receptor; GRE/MRE, glucocorticoid/mineralocorticoid response element; H3, histone 3; hnRNA, heteronuclear RNA; HS, half site; *Klf9*, Krüppel-like factor 9; KSM, *Klf9* synergy module; lncRNA, long noncoding RNA; LPS, lipopolysaccharide; NFκB, nuclear factor κB; NR, nuclear hormone receptor; NRS, normal rabbit serum; p50, NFκB p50 subunit; PND, postnatal day; pol II, polymerase II; RE, restriction enzyme; *rpL8*, ribosomal protein L8; RT-qPCR, real-time quantitative PCR; RXR, retinoid X receptor; S5P, serine 5 phosphorylated; shRNA, small hairpin RNA; TF, transcription factor; TH, thyroid hormone; TR, TH receptor; T_3RE, T_3 response element; *TRPM3*, transient receptor potential cation channel M3; TSS, transcription start site.

TH and GC act via ligand-activated transcription factors (TFs) (nuclear hormone receptors [NRs]) (11). Synergistic interactions among TFs during animal development help to establish cellular competency, or may enhance sensitivity to developmental signals that vary in space and time (12).

We recently found that the Krüppel-like factor 9 (*Klf9*) gene is synergistically transactivated by TH plus GC (see also Ref. 13), it is a direct genomic target for TH receptor (TR) and GC receptor (GR), and it exhibits strong developmental and hormone-dependent regulation in *Xenopus* and mouse central nervous systems (14–25). *Klf9* mediates TH actions on neuronal (15, 16, 26–30) and oligodendrocyte differentiation (28), and *Klf9*-deficient mice show defects in cerebellar Purkinje cell development, delayed neuronal maturation, impaired neurogenesis-dependent long-term potentiation in the dentate gyrus, and impaired behavior consistent with defects in these brain areas (31, 32). Given its strong hormone regulation, and its demonstrated roles in development, *Klf9* may represent a key regulatory node for hormone synergy on phenotypic expression (25).

In the current study we investigated the molecular basis for synergistic transactivation of *Klf9* by TH and GC as a model to understand NR synergy. We discovered an ultraconserved enhancer element of approximately 180 bp located 4–6 kb upstream of the transcription start sites (TSSs) of tetrapod *Klf9* genes that supports hormone synergy (*Klf9* synergy module [KSM]). We show that liganded TR modulates GR recruitment to the KSM and that combined hormone treatment increases serine 5 phosphorylated (S5P) RNA polymerase II (pol II) at the KSM, which leads to the production of enhancer RNAs (eRNAs). We also found that the KSM interacts with the *Klf9* promoter and far upstream regions through chromosome looping, and these interactions may be important for KSM enhancer function.

Materials and Methods

Animal care

Early prometamorphic *Xenopus tropicalis* tadpoles at Nieuwkoop-Faber (33) stages 52–54 were obtained from in-house spawns and maintained in 150-L holding tanks at 23°C on a 12-hour light, 12-hour dark photoperiod. For experiments, tadpoles were transferred to 4-L aquaria (6 tadpoles/aquarium at a density of 2 tadpoles/L; Aquatic Habitats) and treated with vehicle (0.005% dimethylsulfoxide [DMSO] + 0.001% ethanol [EtOH]) or hormones added directly to the aquarium water: T_3 (1nM, 5nM, or 50nM; T2877; Sigma) and corticosterone (CORT) (100nM; C2505; Sigma). Hormones were replenished at 12 hours and treatment continued for an additional 12 hours. Animals were euthanized by immersion in 0.1% benzocaine (Sigma), the brains microdissected, and the region of the diencephalon was collected for RNA isolation and gene expression analysis by real-time quantitative PCR (RT-qPCR) (see below).

We purchased adult wild-type C57/BL6J mice from The Jackson Laboratory, maintained them on a 12-hour light, 12-hour dark photoperiod, provided food and water ad libitum, and bred them in the laboratory to generate offspring for analysis. We administered hormone injections and then conducted gene expression analysis by RT-qPCR, or chromatin immunoprecipitation (ChIP) assays (described below) on microdissected hippocampal region of the brain. For gene expression analysis, we administered intraperitoneal (ip) injections at postnatal day (PND)6 of vehicle (corn oil + EtOH), T_3 (25 μg/kg BW) (17), CORT (14 mg/kg BW) (18), or T_3 plus CORT. The T_3 and CORT were first dissolved in EtOH at high concentration and then added dropwise to corn oil with vigorous mixing (final concentration 0.05% EtOH). A separate group of control animals was not injected and not handled. One hour after injection, animals were killed and brains collected for gene expression analysis. For TR ChIP assay we gave ip injections to PND5 mice of vehicle (0.9% saline, 0.05% EtOH) or T_3 (25 μg/kg BW) and collected brains 4 hours after injection (17). For GR ChIP assay 1 group of PND6 mice was unhandled (unstressed control) and another received ip injections of CORT (14 mg/kg BW) and killed 4 hours later (18). All animal experiments were conducted in accordance with the guidelines of the University Committee on the Care and use of Animals at the University of Michigan.

RNA extraction, reverse transcription and RT-qPCR

We extracted total RNA from tadpole and mouse brain, and tissue culture cells using TRIzol reagent (Invitrogen). One microgram of total RNA was used for cDNA synthesis using the High Capacity Reverse Transcription kit with ribonuclease inhibitor from Applied Biosystems (Life Technologies Corp). For quantitative PCR we designed TaqMan assays and conducted RT-qPCR using an ABI 7500 fast real-time PCR machine with Absolute qPCR low ROX Mix (ABgene). The primers and TaqMan probes used to analyze *Klf9* and *Med1* mRNAs spanned exon/intron boundaries (Supplemental Table 1). Standard curves were constructed using cDNA pools to compare relative expression levels. *Klf9* mRNA levels were normalized to *Gapdh* mRNA in mouse cells (Applied Biosystems assay 4331182) or to ribosomal protein L8 (*rpL8*) in frog cells (34). The *Gapdh* or *rpL8* mRNA levels did not change with any of the treatments (data not shown). To measure *Klf9* heteronuclear RNA (hnRNA) or enhancer RNA we treated total RNA with DNAse I (20 U; Roche) before cDNA synthesis and designed TaqMan assays to target the single *Klf9* intron or the KSM, respectively (Supplemental Table 1). In all cases, we confirmed that RT-qPCR without reverse transcriptase did not yield amplicons (data not shown). To determine the direction of *Klf9* eRNA synthesis, strand-specific primers (Supplemental Table 1) were used for cDNA synthesis followed by semiquantitative PCR (Supplemental Materials and Methods).

Plasmid constructs

One-kilobase fragments from 0 to −7 kb upstream of the *X. tropicalis Klf9* TSS were PCR amplified from genomic DNA (Supplemental Table 2). We also PCR amplified the evolutionarily conserved upstream regions of the mouse and frog *Klf9*

gene (KSM, described in Results; mouse: 179 bp from −5333 to −5154 bp; frog: 164 bp from −6000 to −5836 bp upstream of TSS). The PCR fragments were cloned into the pGL4.23 promoter-luciferase reporter vector at the *Xho*I and *Hin*dIII sites to generate plasmids containing the mouse or frog KSM region. Single or multiple nucleotide substitutions within the predicted NR half sites (HSs) (see below) of the mouse KSM were introduced using the QuikChange Site-Directed Mutagenesis kit (Stratagene) following the manufacturer's protocol.

Cell culture and transient transfection assays

Xenopus laevis embryonic fibroblast (XTC-2) and renal epithelium (A6)-derived cell lines were cultured at 25°C under an atmosphere of 5% CO_2 in Leibovitz L-15 medium (diluted 1:1.5) supplemented with sodium bicarbonate (2.2 g/L), penicillin G (100 U/mL), streptomycin sulfate (100 μg/mL), and 10% fetal bovine serum (FBS). Before initiating hormone treatments, the growth medium was changed to L-15 medium with FBS that had been stripped of thyroid (35) and steroid hormones (36).

The HT-22 cell line was derived from mouse hippocampus and immortalized with the Simian virus 40 T antigen (37, 38). This line exhibits properties of differentiated neurons, eg, they express neuron specific markers such as enolase and the neurofilament triplet but not the glial cell marker, glial fibrillary acidic protein (37–40). It expresses mRNAs for GR and MR, but only the GR is translated into a functional protein (18). We cultured HT-22 cells at 37°C under an atmosphere of 5% CO_2 in DMEM (Invitrogen) containing sodium bicarbonate (2.2 g/L), penicillin G (100 U/mL)/streptomycin sulfate (100 μg/mL), and 10% FBS. Before initiating hormone treatments, the growth medium was changed to DMEM with hormone-stripped FBS.

For gene expression analysis we seeded cells at a density of 2.5×10^6 cells per well in 6-well plates. When cells reached 80% confluency, and immediately before hormone treatments, we replaced the growth medium with serum-free L-15 (XTC-2 and A6) or DMEM (HT-22). The T_3 was dissolved in DMSO and CORT in 100% EtOH and added to the medium to the final concentrations indicated below. Control treatments received an equivalent concentration of vehicle (0.03% DMSO, 0.001% EtOH). To induce nuclear factor κB (NFκB) signaling, we treated HT-22 cells with 1 mg/mL of lipopolysaccharide (LPS) (L3012; Sigma) for 20 hours and then treated with T_3 (30nM), CORT (100nM), or T_3 plus CORT. All hormone treatments were continued for 4 hours before cell harvest for RNA extraction or dual luciferase assay. Gene expression experiments were repeated at least 3 times with 3–6 replicate wells per treatment.

For luciferase reporter experiments we seeded cells at 6.5×10^4 cells per well in 24-well plates in growth medium and transfected at 50%–60% confluency with 250 ng of the pGL4.23 reporter constructs plus 20 ng of p*Renilla* plasmid using the FuGENE 6 transfection reagent (Roche) following the manufacturer's protocol. Immediately before transfection the growth medium was replaced with medium containing hormone-stripped FBS without penicillin/streptomycin, and cells were incubated with the transfection mixture overnight. Cells were then treated in serum-free medium with vehicle (0.03% DMSO, 0.001% EtOH), T_3 (30nM), CORT (100nM), or T_3 plus CORT for 4 hours before harvest for luciferase activity using the Dual Luciferase Assay System (Promega). Firefly luciferase activity was quantified using a luminometer (Femtometer FB 12; Zylux Corp) and normalized to *Renilla* luciferase activity. Each transfection experiment was conducted at least 3 times with 4–5 wells per treatment.

Electrophoretic mobility shift assay

We conducted EMSA as described by Hoopfer et al (24) with recombinant *X. laevis* TRβ and retinoid X receptor (RXR)α, and human GR that we synthesized in vitro using the TnT SP6 quick-coupled translation system (Promega). We programmed the reactions with 1 μg of pSP76-xTRβ, pSP76-xRXRα (gifts of Yun-Bo Shi) or CMV-hGR (OriGene) plasmids and confirmed protein expression by [^{35}S]-labeled amino acid incorporation, SDS-PAGE, and autoradiography (24). Wild-type and mutant duplex oligonucleotides corresponding to the predicted direct repeat with 4-base spacer (DR+4) T_3 response element (T_3RE), the GRE/MRE (at −5.3 kb from the TSS) (18), and predicted HSs 3–5 located within the mouse KSM, and the upstream GRE/MRE (at −6.1 kb from the TSS) (18) (Supplemental Table 2) were labeled with ^{32}P-dCTP by Klenow fill-in for use as probes in EMSA.

ChIP assay

We isolated chromatin from HT-22 cells treated with vehicle (EtOH + DMSO), T_3 (30nM), CORT (100nM), or T_3 plus CORT. We also isolated chromatin from the hippocampal region of PND6 mice 1 hour after injection of vehicle (oil), or CORT (14 mg/kg); a group of control animals was left unhandled. Five micrograms of sheared chromatin were used for each reaction, and ChIP assays were conducted as described by Denver and Williamson (17). We used a rabbit polyclonal antiserum raised against the full-length *X. laevis* TRβ (PB antiserum, 5 μL; it does not distinguish TRα from TRβ; provided by Yun-Bo Shi). This antiserum has been used extensively for ChIP assay on frog tissues (41–43) and in mouse (17, 44). The frog and mouse TR proteins share greater than 90% sequence identity. We also used commercial antibodies to mouse GR (5 μg; M-20X; Santa Cruz Biotechnology, Inc), RNA pol II C-terminal domain (2 μg; 5408; Abcam), S5P pol II (2 μg; 5131–50; Abcam), S2P pol II (2 μg; 5095; Abcam), NFκB p50 subunit (p50) (3 μg; 7971; Abcam), histone 3 (H3) (5 μL; 06–755; Millipore), acetylated H3 (acH3) (5 μL; 06–599 Millipore), acH4 (5 μL; 06–866; Millipore), or normal rabbit serum (NRS) (Sigma). We also used ChIP samples that were prepared previously by Denver and Williamson (17) from PND5 vehicle or T_3-injected mouse brain, and vehicle or T_3-treated N2a[TRβ] cells. We analyzed ChIP DNA by quantitative real-time PCR using TaqMan primer/probe sets that targeted different regions of the mouse *Klf9* gene (Supplemental Table 1). Each of the TaqMan primer/probe sets had similar PCR efficiency.

Chromosome interaction analysis by paired end tag sequencing (ChIA-PET)

The ChIA-PET method allows for determination of protein-DNA binding sites and the physical interactions between nuclear proteins supported by chromosomal looping (45, 46). We treated Nieuwkoop-Faber stage 50 *X. tropicalis* tadpoles with 10nM T_3 for 24 hours, isolated chromatin from a pool of 8 tail fins, and conducted ChIP and ChIA-PET following our published methods (45, 47–49). Briefly, long-range chromatin interactions were captured by DNA-protein cross-linking with formaldehyde. Chromatin was fragmented by sonication, and

DNA-protein complexes were enriched by ChIP using polyclonal antiserum against *X. tropicalis* TR. Tethered DNA fragments were connected with DNA linkers by proximity ligation. The ligation generated 2 types of products: self-ligation of the same DNA fragments and interligation between different DNA fragments in individual chromatin complexes. Short tag signature information (20–30 bp) from the 2 ends of target DNA fragments (PETs) was extracted by restriction enzyme (RE) digestion. The PETs were sequenced on the SOLiD platform. The resulting ChIA-PET sequences were mapped to the reference *X. tropicalis* genome. Self-ligation PET sequences were mapped in the reference genome within a 3-kb span, demarcating ChIP DNA fragments, similar to the standard ChIP-sequencing method. Interligation PET sequences reveal close spatial proximity through chromatin looping. Singleton PETs are presumed to be experimental noise, and overlapping PET clusters are considered enriched putative binding sites or interaction events. Full details of the experimental procedures and the complete datasets generated by ChIA-PET applied to *X. tropicalis* will be published elsewhere.

Chromosomal conformation capture (3C)-qPCR assay

We conducted 3C-qPCR assay on chromatin isolated from HT-22 cells as described by Hagège et al (50) with minor modifications. We plated HT-22 cells in 10-cm dishes in DMEM with 10% hormone-stripped FBS. After 48 hours, cells were treated with 30nM T_3 plus 100nM CORT for 4 hours, and single cell suspensions were prepared as previously described (50). Cross-linking of protein and DNA was done by gently tumbling cells in 10-mL PBS with 10% hormone-stripped FBS and 2% formaldehyde at room temperature for 10 minutes. A second protein-protein cross-linking step was conducted by tumbling cells in 10-mL PBS with 10% hormone-stripped FBS and 0.2mM dithiobissuccinimidylpropionate (Pierce Chemical Co) for 10 minutes at room temperature. Cells were then pelleted, resuspended in ice-cold lysis buffer (10mM Tris-HCl [pH 7.5], 10mM NaCl, 5mM $MgCl_2$, 0.1mM EGTA, and 1× protease inhibitor), and incubated on ice for 10 minutes. Cell nuclei were pelleted, resuspended in 0.5 mL of 1.2× RE (*Dpn*II buffer and New England Biolabs buffer 2) buffer with 7.5 μL of 20% sodium dodecyl sulfate, and incubated for 1 hour at 37°C with shaking at 900 rpm. Triton X-100 (Sigma) was added at a final concentration of 2% and incubated for 1 hour at 37°C with shaking at 900 rpm.

Four hundred units of *Dpn*II or *Hin*dIII (New England Biolabs) were added, and the incubation continued for 1 hour at 37°C with shaking. The chromatin digested with *Hin*dIII served as a negative control. Restriction enzymes were inactivated by incubating samples at 65°C for 25 minutes. Digested nuclei were transferred to a 50-mL falcon tube, and ligation was conducted by adding 100 U of T_4 DNA ligase (New England Biolabs) in a final volume of 6.5 mL of 1.15× ligation buffer (10× ligation buffer, 660mM Tris-HCl [pH 7.5], 50mM dithiothreitol, 50mM $MgCl_2$, and 10mM ATP). In this large volume, RE-digested fragments that interact within a protein complex have a higher chance of becoming ligated than random RE-digested fragments. The presence of ligated fragments indicates a positive long-range interaction between genomic regions. Ligated samples were treated with proteinase K and reverse cross-linked at 65°C overnight. DNA was purified by phenol-chloroform extraction and EtOH precipitation.

As a control for template and primer efficiency, a bacterial artificial chromosome clone containing the mouse *Klf9* locus was similarly digested with *Dpn*II, ligated and purified by phenol-chloroform extraction. Sample purity and loading adjustments for qPCR were conducted as described in Hagège et al (50).

Positive interactions, as indicated by the presence of ligated chromatin fragments, were detected by the presence of qPCR amplicons (80–120 bp in length) using a constant reverse primer and a TaqMan probe targeted to the mouse *Klf9* promoter, and forward primers targeted within 50 bp of *Dpn*II cutting sites at several genomic region covering 10 kb upstream of the TSS (Supplemental Table 3). The *Hin*dIII-digested and ligated chromatin fragments served as a negative control for qPCR amplification because the combination of different forward primers (designed close to a *Dpn*II cutting site) and the constant reverse primer and TaqMan probe, should yield amplicons more than 800 bp, which are beyond the limit of detection of the qPCR assay. We express the data based on positive interactions for 8 independent samples (4 vehicle and 4 hormone-treated samples) as detected by the presence of amplification products by qPCR.

Data analysis and statistics

Data were analyzed by one-way ANOVA or Student's *t* test using SYSTAT ($\alpha < 0.05$; version 10; SPSS Inc). Derived values from dual luciferase and ChIP assays were $\log_{10}$ transformed before statistical analysis. A synergistic effect of T_3 and CORT on gene expression and ChIP signal is defined as: 1) a greater than additive effect by one standard deviation with combined hormone treatment, or 2) no effect with T_3 or CORT alone but a significant effect with combined hormone treatment (2). To predict putative TF binding sites we used the online programs Transcription Element Search System (www.cbil.upenn.edu/tess) and Match (www.gene-regulation.com/pub/programs.html#match) using a library of matrices from TRANSFAC 6.0 (www.gene-regulation.com) with core and matrix similarity of TF binding sites set higher than 0.85. The conservation of the identified TF binding sites and flanking sequences was assessed using BLAT (http://genome.ucsc.edu/). Extracted sequences were aligned using Clustal W. The percent similarity to human was calculated for the T_3RE and GRE/MRE HS, and nucleotide frequency diagrams were produced with Weblogo (http://weblogo.berkeley.edu/logo.cgi).

Results

Synergistic transactivation of the *Klf9* gene by T_3 plus CORT

Treatment of XTC-2 or A6 cells with T_3 or CORT for 4 hours increased *Klf9* mRNA above control, whereas combined hormone treatment caused synergistic increases, with the largest effect (53-fold increase) seen in A6 cells (Figure 1A). In HT-22 cells T_3 and CORT also independently and synergistically increased *Klf9* mRNA.

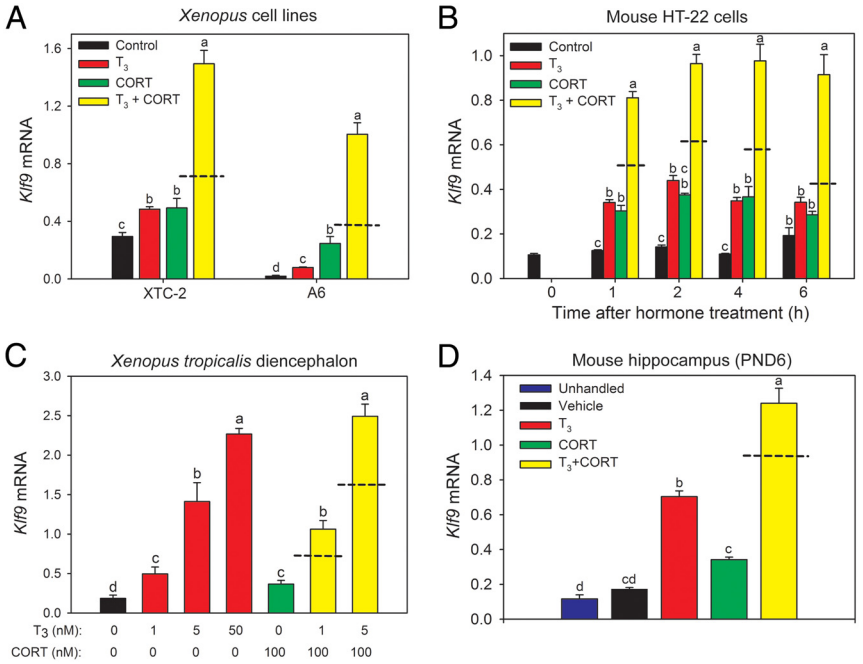

Figure 1. TH and CORT act synergistically to induce *Klf9* mRNA in frog and mouse. A, Hormone-dependent *Klf9* gene expression in *X. laevis* cell lines. We treated the *X. laevis* embryonic fibroblast (XTC-2) and renal epithelium (A6)-derived cell lines (n = 4–6/treatment) with vehicle, T_3 (5nM), CORT (100nM), or T_3 plus CORT for 4 hours before harvesting for RNA isolation. Hormone treatment caused statistically significant increases in *Klf9* mRNA in both cell lines. XTC-2, T_3: 1.6-fold; CORT: 1.6-fold; T_3 + CORT: 5-fold; $F_{(3,15)} = 85.01$, $P < .01$; A6, T_3: 4-fold; CORT: 12-fold; T_3 + CORT: 53-fold; $F_{(3,15)} = 93.59$, $P < .01$; ANOVA. B, Hormone-dependent *Klf9* gene expression in the mouse hippocampus-derived cell line HT-22. We treated HT-22 cells (n = 4–6/treatment) with vehicle, T_3 (30nM), CORT (100nM), or T_3 plus CORT for different times before harvesting for RNA extraction. Hormone treatment caused statistically significant increases in *Klf9* mRNA ($F_{(3,15)} = 42.36$, $P < .001$; ANOVA): T_3: 2.4-fold; CORT: 2.7-fold; T_3 + CORT: 6.5-fold; 1 hour: $F_{(3,15)} = 216.5$, $P < .001$; 2 hours: $F_{(3,15)} = 17.6$, $P < .01$; 4 hours: $F_{(3,15)} = 68.26$, $P < .001$; 6 hours. C, Hormone-dependent *Klf9* gene expression in early prometamorphic (Nieuwkoop-Faber stage 52–54) *X. tropicalis* tadpole brain (diencephalon). We treated tadpoles (n = 6/treatment) with T_3 and CORT at the doses indicated in the graph for 24 hours (hormones replenished at 12 hours), collected brains and microdissected the diencephalon for RNA extraction. Hormone treatment caused statistically significant increases in *Klf9* mRNA ($F_{(6,\ 41)} = 47.99$, $P < .001$; ANOVA): 1nM T_3: 2.67-fold; 100nM CORT: 2-fold; 1nM T_3 + 100nM CORT: 5.75-fold; 5nM T_3 + 100nM CORT: 13.5-fold. D, Hormone-dependent *Klf9* gene expression in the hippocampus of PND6 wild-type C57/BL6J mice. Mice were left unhandled, or were given ip injections of vehicle (corn oil + EtOH 0.05%), T_3 (25 μg/kg BW), CORT (14 mg/kg BW), or T_3 plus CORT. One hour after injection, mice were killed, and the hippocampal region was dissected for RNA extraction (n = 5–6/ treatment). Hormone treatment caused statistically significant increases in *Klf9* mRNA ($F_{(4,\ 25)} = 121.4$, $P < .01$; ANOVA): T_3: 3-fold; CORT: 1.5-fold; T_3 plus CORT: 7-fold. In all experiments, total RNA was analyzed for *Klf9* mRNA levels by RT-qPCR using TaqMan assays. The *Klf9* mRNA levels were normalized to the reference genes *rpL8* (frog) and *Gapdh* (mouse), which were unaffected by hormone treatment (data not shown). Tissue culture experiments were repeated 3–4 times. Bars represent the mean ± SEM, and letters above the means indicate significant differences among treatments (means with the same letter are not significantly different; Tukey's multiple comparison test; $P < .05$). Dashed lines indicate the calculated additive effect of combined hormone treatment.

The synergistic effect was seen at 1 hour and persisted through 6 hours of hormone treatment (Figure 1B).

We also saw hormone synergy on *Klf9* hnRNA in HT-22 cells, supporting increased gene transcription (Supplemental Figure 1). Treatment with the protein synthesis inhibitor cycloheximide (CHX) (Supplemental Materials and Methods) did not affect hormone-dependent induction of *Klf9* mRNA in either XTC-2 or HT-22 cells which also supports direct hormone action on *Klf9* gene transcription (Supplemental Figure 2).

We next investigated whether hormone synergy occurs on *Klf9* in tadpole and mouse brain in vivo. Treatment with T_3 or CORT alone increased *Klf9* mRNA in tadpole brain, whereas combined hormone treatment caused a synergistic increase (Figure 1C). In mouse, ip injection of T_3 or CORT alone increased *Klf9* mRNA in the hippocampal region of the brain 1 hour after injection, whereas combined hormone treatment caused a synergistic increase (Figure 1D).

An evolutionarily conserved approximately 180-bp genomic region located upstream of tetrapod *Klf9* genes supports synergistic transactivation by T_3 plus CORT

To identify genomic regions that confer hormone-dependent synergistic transactivation of *Klf9*, we used promoter-reporter assays in XTC-2 cells to screen 1-kb fragments of the *X. tropicalis Klf9* 5′-flanking region covering 0 to −7 kb upstream of the TSS. We found that the fragment located −5 to −6 kb upstream of the TSS was T_3 and CORT-responsive, and this region supported synergistic transactivation (Figure 2A; see also Supplemental Figure 3 for HT-22 cells).

Bioinformatics analysis revealed an approximately 180-bp segment within the −5- to −6-kb fragment that is highly conserved among tetrapod *Klf9* genes (Figure 2B and Supplemental Tables 4 and 5). We found orthologous sequences in most tetrapod genomes, and comparative sequence analysis showed that this intergenic region is remarkably conserved among tetrapods, eg, sequence similarity was 100% between human and chimp and 75% between human and frog (Supplemental Table 6). Sequence similarity within the coding regions of tetrapod *Klf9* genes was sim-

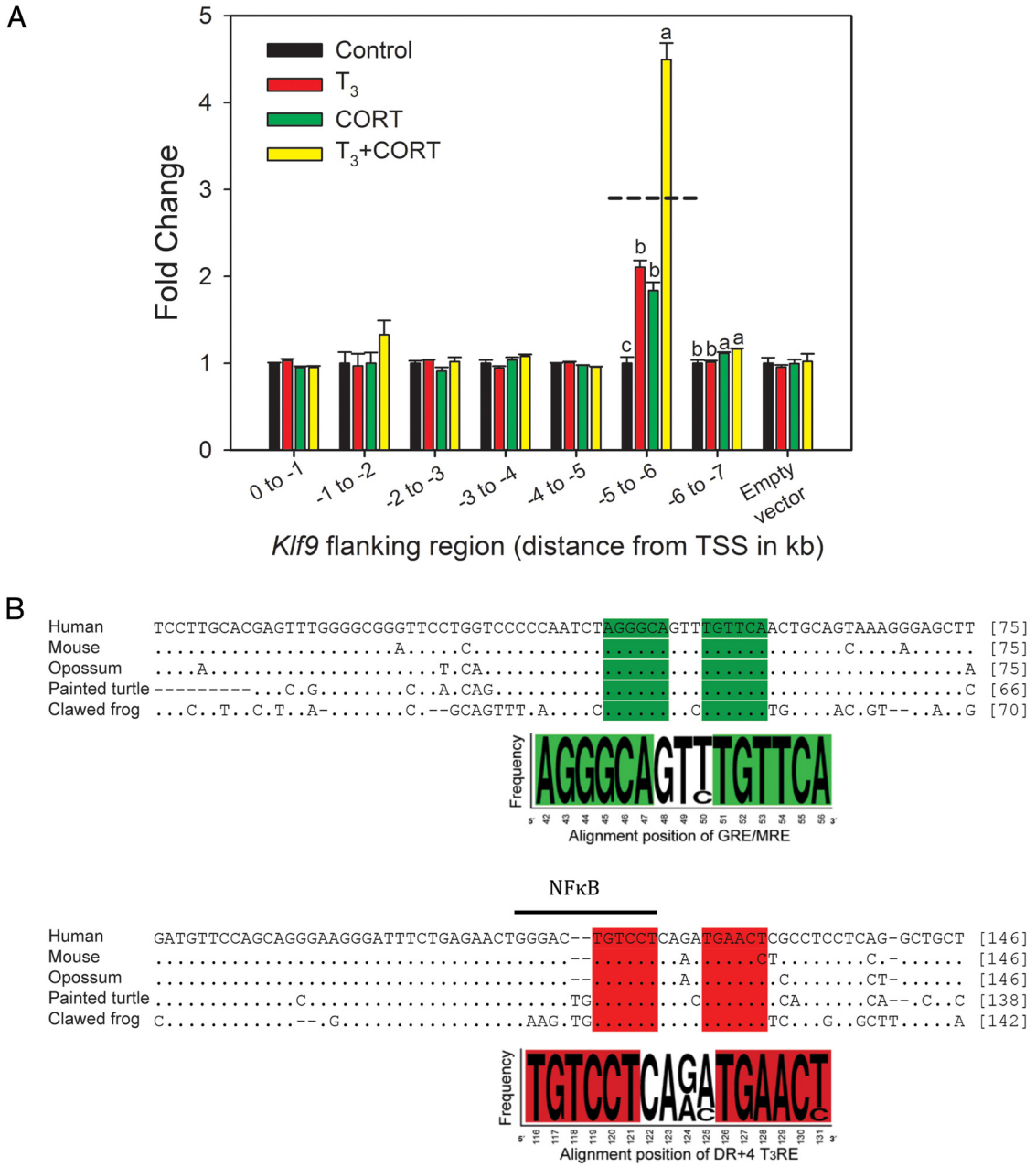

Figure 2. Identification of an evolutionarily conserved approximately 180-bp genomic region upstream of tetrapod *Klf9* genes that supports synergistic transactivation by TH and CORT. A, Enhancer-reporter scan of the 5′-flanking region of the *X. tropicalis Klf9* gene; 1-kb fragments covering 0 to −7 kb upstream of the *Klf9* TSS were cloned into the luciferase vector pGL4.23 and transfected into XTC-2 cells. We treated cells with vehicle (0.03% DMSO, 0.001% EtOH), T_3 (5nM), CORT (100nM), or T_3 plus CORT for 4 hours before harvest and analysis by dual luciferase assay. The −5- to −6-kb fragment supported individual hormone responses and hormone synergy ($F_{(3,15)} = 89.44$, $P < .001$; ANOVA). The −6- to −7-kb fragment showed a small response to CORT ($F_{(3,15)} = 11.64$, $P < .05$; ANOVA) that was unaffected by T_3. Bars represent the mean ± SEM (n = 4–5/treatment) fold change, and letters above the means indicate significant differences among hormone treatments within a promoter fragment (means with the same letter are not significantly different; Tukey's multiple comparison test; $P < .05$). The dashed line indicates the calculated additive effect of combined hormone treatment. B, A genomic region spanning approximately 180 bp upstream of tetrapod *Klf9* genes is evolutionarily conserved (the KSM). Shown is the most highly conserved region spanning 138–146 nt for 5 tetrapods (see Supplemental Tables 4 and 5 for more comprehensive analyses). The highlighted sequences show the highly conserved GRE/MRE and DR+4 T_3RE regions. The evolutionarily conserved, predicted NFκB site that overlaps with the T_3RE is indicated by a bar over the sequence. Note that there is a 2-base insertion in nonmammalian tetrapods. Genomic location of the KSM relative to the TSS for species for which it was possible to determine: *X. tropicalis*: −6000 to −5836 bp; mouse: −5333 to −5154 bp; human: −4634 to −4505.

ilar to the approximately 180-bp segment. However, sequence similarity among *Klf9* core promoter regions was lower than at the approximately 180-bp segment (Supplemental Table 5). Regional genomic conservation of the *Klf9* locus between human and vertebrates was analyzed using the University of California Santa

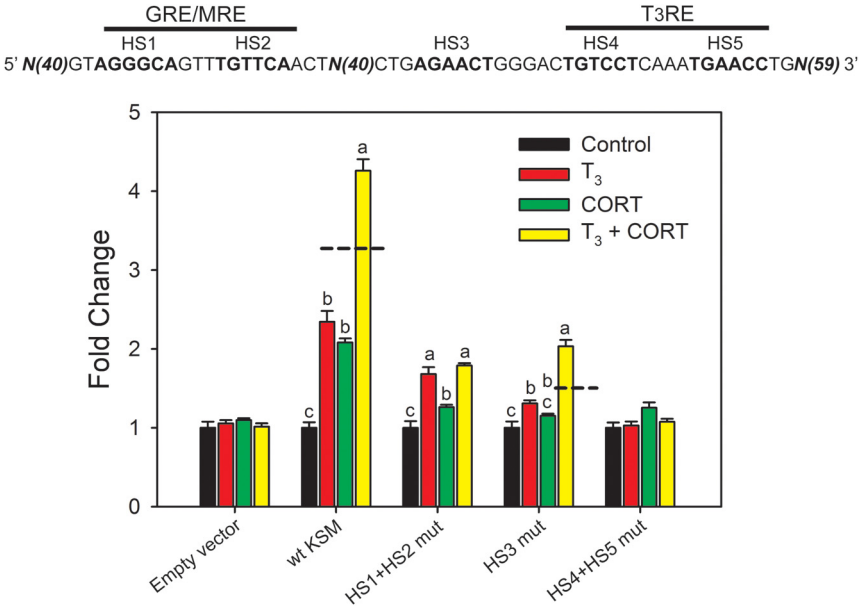

Figure 3. Site-directed mutagenesis of the mouse KSM-identified DNA sequences required for individual and synergistic hormone responses. We subcloned a 179-bp fragment corresponding to the mouse KSM into the luciferase reporter vector pGL4.23 and introduced mutations into predicted hormone response element HS (shown above the graph) by site-directed mutagenesis (Supplemental Table 2). The constructs were transfected into HT-22 cells, and cells were treated with vehicle (0.03% DMSO, 0.001% EtOH), T_3 (30nM), CORT (100nM), or T_3 plus CORT for 4 hours before harvest and analysis by dual luciferase assay. Bars represent the mean ± SEM (n = 4/treatment), and letters above the means indicate significant differences among treatments (means with the same letter are not significantly different; Tukey's multiple comparison test, $P < .05$). Dashed lines indicate the calculated additive effect of combined hormone treatment.

Cruz Genome Browser and is shown in Supplemental Figure 4.

To determine whether the evolutionarily conserved approximately 180-bp region could support synergistic transactivation we subcloned the mouse *Klf9* fragment (179 bp) into pGL4.23 and conducted promoter-luciferase assays in HT-22 cells. This genomic sequence supported independent and synergistic transactivation by T_3 and CORT (Figure 3). We therefore designate this region the KSM. The orthologous region of the frog *Klf9* locus also supported independent and synergistic transactivation by T_3 and CORT in XTC-2 cells (Supplemental Figure 5A). The T_3RE in this region also functions in vivo as determined by electroporation-mediated gene transfer into tadpole brain and dual luciferase assay (Supplemental Figure 5B and Supplemental Materials and Methods) (see also Ref. 51).

Genomic location, structural features, and evolutionary conservation of tetrapod KSMs

Tetrapod KSMs are located in an intergenic region between *Klf9* and the transient receptor potential cation channel M3 (*TRPM3*) gene (Supplemental Figure 6); these genes are in opposite orientation on human chromosome 9 (mouse chromosome 19). The *Klf9* and *TRPM3* genes are present and adjacent in all jawed vertebrates. We were unable to locate any genomic regions orthologous to the KSM between *Klf9* and *TRPM3* in any other jawed vertebrates, or elsewhere in the genomes of any vertebrates (Supplemental Figure 6). This includes global and local searches in the genomes of the coelacanth, several actinopterygians, horn shark, lamprey, lancelet, and tunicate. Taken together, our findings support that the KSM originated in the *Klf9*/*TRPM3* intergenic region before the divergence of modern tetrapods and has been maintained for at least 350 million years.

Mutational analysis identified T_3 and CORT response elements required for hormone synergy within the mouse KSM

We previously identified a functional GRE/MRE in the region of the mouse KSM (−5.3 kb relative to the TSS; Figures 2B and 3, comprised of HS1 and HS2) that is conserved from frog (*X. tropicalis*; −5.96 kb) to human (−4.63 kb) (18). Furlow and Kanamori (23) previously identified a DR+4 T_3RE at approximately −6.0 kb relative to the *Klf9* TSS in *X. laevis*. A conserved T_3RE is located within the KSM of *X. tropicalis* (−5.90 kb), mouse (−5.23 kb) (19), and human (−4.57 kb) (Figures 2B and 3, comprised of HS4 and HS5). Transcription Element Search System analysis of this conserved approximately 180-bp region identified another highly conserved sequence predicted to be a GRE/MRE HS (HS3) (Figure 3). However, this sequence was not protected by GR in a DNAse I footprinting assay (18).

Mutation of both HSs of the GRE/MRE (HS1+HS2 mut) attenuated, but did not eliminate, the CORT response (see also Ref. 18), attenuated the T_3 response, and eliminated hormone synergy (Figure 3). Mutation of the predicted GRE/MRE HS3 (HS3 mut) abolished the CORT response (with the −5.3-kb GRE/MRE intact) and reduced, but did not eliminate, the T_3 response and hormone synergy. DNAse I protection assay (18) and EMSA (discussed below) showed that GR does not bind this sequence; a protein required for CORT response likely binds HS3, but we currently do not know its identity.

Mutation of both HSs of the predicted T_3RE (HS4+HS5 mut) eliminated all hormone responses.

TR and GR bind to the mouse KSM in vitro

Using EMSA we found that TR-RXR heterodimers bound a probe containing the predicted T_3RE within the mouse KSM (Figure 4A). Mutation of the 5′ T_3RE HS (HS4) reduced, whereas mutation of both HSs eliminated TR-RXR binding (Figure 4A). Because the KSM reporter with a mutated 3′ T_3RE HS (HS5) retained some T_3 responsiveness (and hormone synergy; data not shown), we investigated whether TR-RXR could bind a probe containing only the predicted HSs HS3 and HS4. However, TR-RXR was unable to bind this DNA sequence (Figure 4A).

The GR bound the previously characterized −5.3-kb GRE/MRE (HS1 and HS2) within the KSM, which was competed for by wild-type but not mutant HS1+HS2 radioinert oligonucleotide (Figure 4B) (18). Because the KSM reporter with mutations in both GRE/MRE HSs retained some CORT responsiveness (see above) we investigated whether GR could bind a probe containing HS3–HS5. However, the GR was unable to bind this DNA sequence (18).

In silico analysis identified other TF binding sites in the mouse KSM and at the region of the upstream GRE/MRE (−6.1 kb) and T_3RE (−6.3 kb), which included consensus NFκB sites (18), one of which overlaps with the T_3RE within the KSM (conserved among mammals but with a 2-base insertion in other tetrapods) (Figure 2B and Supplemental Figure 7; see also Supplemental Tables 7 and 8). Using ChIP assay, we found that p50 associated with these regions in HT-22 cell chromatin, and the signal was decreased by treatment with CORT (Supplemental Figure 8A); we did not detect p50 at the mouse *Klf9* intron. Activation of NFκB signaling by LPS enhanced the *Klf9* mRNA response to T_3 in HT-22 cells (Supplemental Figure 8B).

TR and GR associate with the KSM in mouse brain chromatin

ChIP assay for TR on chromatin isolated from the hippocampal region of T_3-injected PND5 mice showed TR association at the KSM (−5.23 kb) (Figure 4C) and at 2 previously identified T_3REs located at −3.8 kb (17) and −6.2 kb from the TSS (see Supplemental Table 9) (19). The TR ChIP signal was significantly greater than the control (ChIP with NRS) at the KSM and the regions of the −3.8 and −6.2 kb T_3REs (although much lower at the −3.8-kb region) but not at a distal intronic site (+11 kb from the TSS) (Figure 4C).

ChIP assay for GR on chromatin extracted from the hippocampal region of PND6 mice 1 hour after ip CORT injection showed CORT-dependent association of GR at the KSM and also at the previously identified GRE/MRE-6.1 located upstream of the KSM (found only in therian mammals) (Figure 4D) (18). By comparison, we detected no significant GR ChIP signal at the distal intron of the mouse *Klf9* gene.

Liganded TR enhances CORT-dependent recruitment of GR, but not TR, across the mouse *Klf9* locus

Analysis of TR and GR association across the *Klf9* locus in HT-22 cells by ChIP assay showed a strong TR signal only at the KSM, which was unaffected by hormone treatment, consistent with TRs being constitutively bound to DNA (Figure 5). We did not see TR association in HT-22 cells at the −3.8-kb T_3RE region that we previously identified in mouse brain and Neuro2a[TRβ1] cells (Figure 4C; although we saw strong TR signal at the KSM in Neuro2a[TRβ1] cells) (17 and data not shown). Also, we did not see TR signal in HT-22 cells at the −6.2-kb T_3RE identified by Chatonnet et al (19) in the mouse cerebellar-derived cell line C17.2 engineered to overexpress TRα1 or TRβ1. Thus, mammalian *Klf9* genes have T_3REs located outside the KSM, which may be used in a tissue and/or developmental-stage dependent manner as compared with the ubiquitous function of the T_3RE within the KSM. The ChIP signal for the NRS control was low to nondetectable across the *Klf9* locus and was not affected by hormone treatment (data not shown).

The GR ChIP signal was low across the *Klf9* locus in HT-22 cells and was not affected by T_3 (Figure 5B). There was a trend towards higher GR signal at the KSM after exposure to CORT but this did not reach statistical significance ($P = .073$). However, combined treatment with T_3 plus CORT caused a robust increase in GR ChIP signal at the KSM and at the −6.1-kb GRE/MRE (Figure 5).

Our GR ChIP assays support that liganded TR promotes recruitment of liganded GR to the *Klf9* locus, thereby enhancing CORT-dependent transcription of the *Klf9* gene. This may represent a key molecular event in the synergistic transcriptional response to hormones. Consistent with this hypothesis, we found that forced expression of a dominant negative TR (dnTR) that does not bind hormone in both HT-22 and XTC-2 cells reduced CORT-dependent induction of *Klf9* mRNA (also reduced the T_3 response and hormone synergy) (Supplemental Materials and Methods and Supplemental Figure 9).

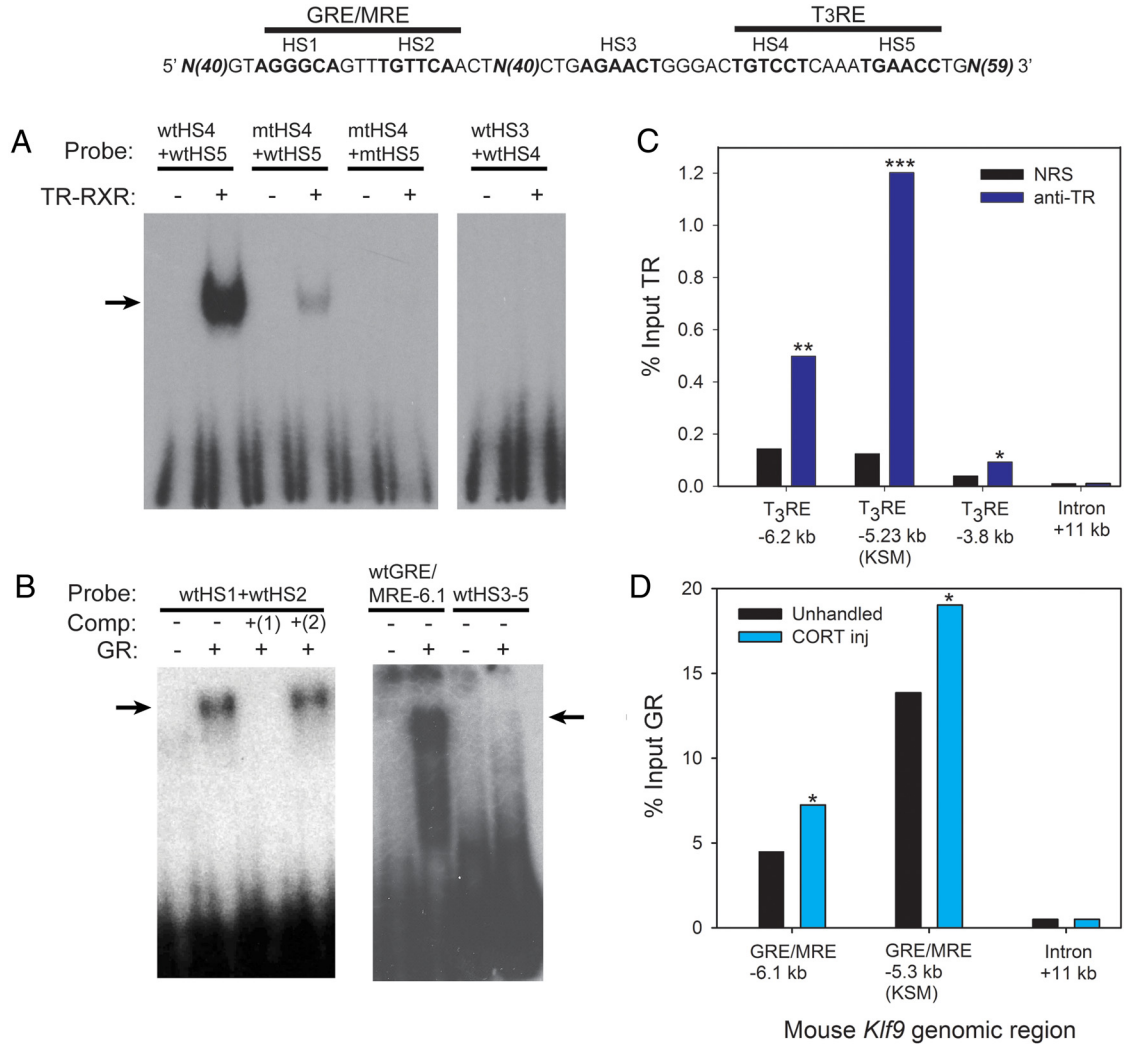

Figure 4. TR and GR bind in vitro to predicted hormone response elements and associate in chromatin with *Klf9* upstream regions in mouse hippocampus. A, EMSA for TR-RXR binding to [^{32}P]-labeled oligonucleotide probes (Supplemental Table 2) corresponding to wild-type (wt) or mutated (mt) hormone response elements located upstream of the mouse *Klf9* gene (shown above the graphs). Probes were incubated with or without in vitro synthesized TRβ plus RXRα before electrophoresis. The arrow indicates supershifted bands due to TR-RXR binding to the radiolabeled probes. The TR-RXR showed strong binding to the wtHS4 + wtHS5 probe (HS, within the KSM shown in the diagram above the graphs), which corresponds to the predicted DR+4 T_3RE located within the KSM, but not to other probes. B, Competitive EMSA for GR binding to [^{32}P]-labeled oligonucleotide probes (Supplemental Table 2) corresponding to wt hormone response elements located at the mouse KSM (at −5.3 kb upstream of the TSS) and the GRE/MRE located upstream of the KSM (at −6.1 kb upstream of the TSS; identified by Bagamasbad et al [18]). Probes were incubated with or without in vitro synthesized GR before electrophoresis. In lanes 3 and 4, the reactions were incubated with 1.5μM radioinert competitor: 1) wtHS1 + wtHS2; 2) mtHS1 + mtHS2. The arrows indicate supershifted bands due to GR binding to the radiolabeled probes. The GR bound to the GRE/MRE-5.3 kb and GRE/MRE-6.1 kb probes but not to the wtHS3–5 probe; GR binding to the GRE/MRE-5.3 kb probe was competed by wt but not by mutant radioinert oligonucleotide. C, TR association at the *Klf9* locus in mouse hippocampus analyzed by ChIP assay. We administered ip injections of vehicle or T_3 (25 μg/kg BW; n = 4–5/treatment) to wt PND5 mice and dissected the hippocampal region 4 hours later for chromatin extraction for TR ChIP assay. We analyzed ChIP DNA by RT-qPCR using TaqMan assays that targeted the region of the predicted T_3RE at −6.2 kb from the *Klf9* TSS, the T_3RE within the KSM (−5.23 kb) and a distal intronic region (+11 kb; negative control region) of the mouse *Klf9* gene. Bars represent the mean ChIP signal expressed as a percentage of input for TR serum (anti-TR) or NRS (negative control). The asterisks indicate statistically significant differences between the anti-TR and NRS groups (*, $P < .05$; **, $P < .01$; ***, $P < .001$; Student's 2 sample *t* test; derived values were $\log_{10}$ transformed before statistical analysis). D, GR association at the *Klf9* locus in mouse hippocampus analyzed by ChIP assay. wtPND6 mice were left unhandled or given ip injections of CORT (14 mg/kg BW; n = 9/treatment). One hour after injection, animals were killed, the hippocampal region was dissected, and chromatin was extracted for GR ChIP assay. The ChIP DNA was analyzed by RT-qPCR using TaqMan assays that targeted the GRE/MRE −6.1 kb, the GRE/MRE at −5.3 kb within the KSM, and a distal intronic region (+11 kb; negative control region) of the mouse *Klf9* gene. Bars represent the mean ChIP signal expressed as a percentage of input. Asterisks indicate statistically significant differences between unhandled and CORT-injected animals ($P < .05$; Student's 2 sample *t* test; derived values were $\log_{10}$ transformed before statistical analysis).

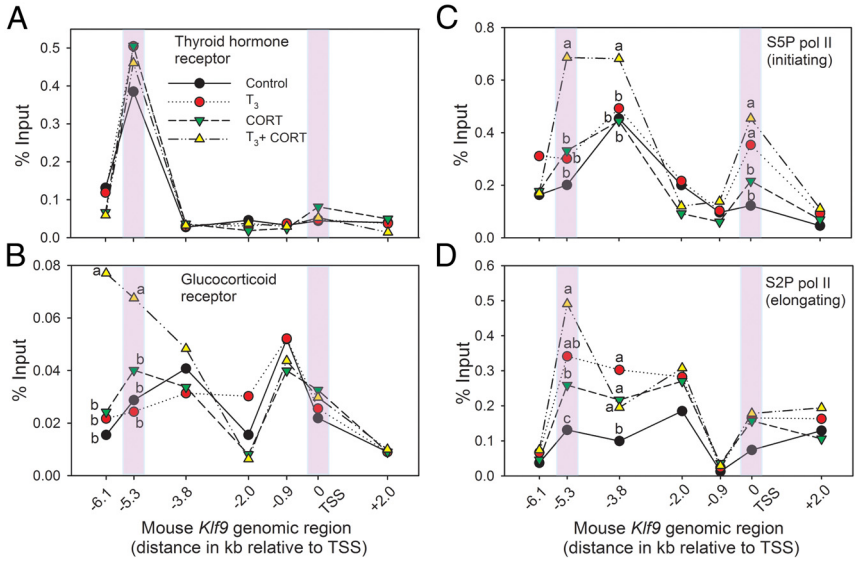

Figure 5. Hormone-dependent recruitment of TR, GR, and S5P (initiating) and S2P (elongating) RNA pol II across the mouse *Klf9* locus. We treated HT-22 cells with vehicle, T_3 (30nM), CORT (100nM), or T_3 plus CORT for 4 hours before harvest for chromatin extraction and ChIP assays. We analyzed ChIP samples (n = 6/treatment) by RT-qPCR using TaqMan assays that targeted different genomic regions of the mouse *Klf9* gene (shown on the x axis, with distances relative to the *Klf9* TSS). Shaded bars highlight the KSM and the TSS. A, Strong TR ChIP signal was seen only at the KSM, but unaffected by hormone treatment. B, The GR ChIP signal was not affected by T_3; CORT increased the mean GR signal, but this did not reach statistical significance (P = .073). Combined hormone treatment increased GR ChIP signal at the KSM ($F_{(3,21)} = 8.631$, $P <$ .001; ANOVA) and at the GRE/MRE-6.1 kb ($F_{(3,21)} = 7.4555$, $P < .05$). C, The S5P pol II ChIP signal peaked at the KSM, −3.8 kb from the TSS, and at the TSS. There were no effects of individual hormone treatments but combined hormone treatment increases S5P pol II signal at the KSM and −3.8 kb (KSM: $F_{(3,18)} = 10.6$, $P < .001$; −3.8 kb: $F_{(3,20)} = 2.43$, $P < .05$; ANOVA). T_3 or T_3 plus CORT increased the S5P pol II signal at the TSS, but CORT alone had no effect ($F_{(3,18)} = 11.31$, $P < .0001$). D, The S2P pol II ChIP signal peaked at the KSM was increased by all hormone treatments, and was highest after combined hormone treatment ($F_{(3,21)} = 6.736$, $P <$ .01). All hormone treatments similarly increased S2P pol II signal at −3.8 kb ($F_{(3,18)} = 3.8$, $P =$ .028). Each point represents the mean, and means with the same letter are not significantly different (ANOVA, Tukey's multiple comparison test; $P < .05$). Absence of letters indicates that there were no statistically significant differences among treatments at that genomic location. Statistical analysis was conducted on $\log_{10}$-transformed data.

Recruitment of RNA pol II across the *Klf9* locus

ChIP assays conducted on chromatin from HT-22 cells showed association of pol II across the mouse *Klf9* locus, but the total pol II signal did not vary by genomic region nor was it affected by hormone treatment (data not shown). We also looked at the association of 2 phosphorylated forms of pol II, S5P, which is involved with transcription initiation, and S2P, which functions in transcription elongation (52, 53). The S5P pol II signal exhibited peaks at the KSM and −3.8 kb from the TSS, and at the TSS (Figure 5). There was no effect of T_3 or CORT alone, but we saw a significant increase in S5P pol II signal at the KSM and at −3.8 kb after combined hormone treatment (ie, a synergistic effect). At the TSS, T_3 alone or T_3 plus CORT increased the S5P pol II signal, but CORT alone had no effect. There were no hormone-dependent changes in S5P pol II signal at the other genomic regions analyzed. The S2P pol II ChIP signal exhibited a peak at the KSM, which was increased by all hormone treatments, but was highest after T_3 plus CORT (Figure 5). All hormone treatments similarly increased S2P pol II signal at −3.8 kb; there were no differences at other genomic regions analyzed.

Hormone treatment causes nucleosome repositioning and histone hyperacetylation at the KSM in HT-22 cells

ChIP assays for H3, acH3, and acH4 showed that T_3 or CORT decreased levels of H3 but increased acH3 (normalized to H3) and acH4 (normalized to H3) at the KSM (Supplemental Figure 10) and −6.1-kb GRE/MRE (data not shown). There was no further enhancement by combined hormone treatment at either genomic region. Hormone treatment did not alter H3, acH3, or acH4 levels at the distal intron (+11 kb from the TSS; data not shown).

The mouse KSM is bidirectionally transcribed to generate long noncoding RNAs (lncRNAs)

The presence of pol II at the KSM prompted us to investigate whether this genomic region is transcribed into RNA. We detected transcripts at the KSM in HT-22 cells and mouse hippocampus (Figure 6; we refer to this RNA as the *Klf9* eRNA). The estimated size of this eRNA is between 1.3 and 4 kb, and it is bidirectionally transcribed (Supplemental Figure 11). The UCSC Genome Browser shows a lncRNA associated with the mouse KSM predicted by Ensembl (54).

In HT-22 cells, the pattern of hormone response of the *Klf9* eRNA was similar to that of the mRNA, but the magnitude of increase in *Klf9* eRNA after combined hormone treatment was significantly greater than the *Klf9* mRNA (Figure 6A; see also Supplemental Figure 11). Similar to the mRNA, the level of *Klf9* eRNA was not affected by protein synthesis inhibition with CHX (Figure 6B). In hippocampus of PND6 mice we saw significant increases in *Klf9* eRNA after T_3 or T_3 plus CORT injection (not synergy) but not with CORT alone ($F_{(4,17)} =$

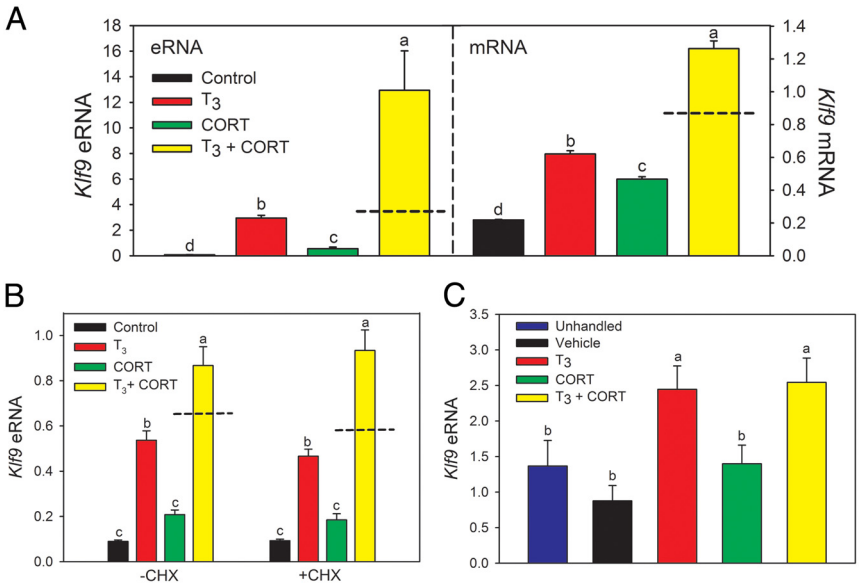

Figure 6. The mouse KSM is transcribed to generate eRNAs, and *Klf9* eRNAs are induced by hormones. A, Hormones induce *Klf9* eRNA in HT-22 cells (left panel). We treated HT-22 cells (n = 4–6/treatment) with vehicle, T_3 (30nM), CORT (100nM), or T_3 plus CORT for 4 hours before harvesting for RNA extraction and analysis of *Klf9* mRNA by RT-qPCR. Shown in the right panel is *Klf9* mRNA analyzed by RT-qPCR in the same samples. There was a 153-fold increase in *Klf9* eRNA induced by combined hormone treatment vs a 6-fold increase in *Klf9* mRNA (eRNA: $F_{(3,11)} = 15.16$, $P < .01$; mRNA: $F_{(3,11)} = 276$, $P < .001$; ANOVA). B, Hormone induction of *Klf9* eRNAs is resistant to protein synthesis inhibition in HT-22 cells. We treated cells with or without CHX (100 μg/mL) for 30 minutes before addition of vehicle, T_3 (30nM), CORT (100nM), or T_3 plus CORT. We continued the incubation for 4 hours before harvest (CHX was present during the 4-h hormone treatment period) and RNA extraction for analysis of eRNAs by RT-qPCR. Hormone induction of *Klf9* eRNAs was unaffected by CHX (−CHX: $F_{(3,15)} = 54.31$, $P < .001$; +CHX: $F_{(3,14)} = 54.87$, $P < .001$). C, Hormones induce *Klf9* eRNAs in mouse brain in vivo. PND6 wild-type mice were left unhandled or were injected ip with vehicle, T_3 (25 μg/kg BW), CORT (14 mg/kg BW), or T_3 plus CORT. One hour after injection, animals were killed, the hippocampal region was dissected, and RNA was extracted for RT-qPCR for eRNAs. There was a significant increase in *Klf9* eRNA after T_3 or T_3+CORT injection (not synergy) but not with CORT alone ($F_{(4,17)} = 5.812$, $P < .05$). In all experiments, both the mRNA and eRNA transcripts were normalized to the mRNA level of the reference gene *Gapdh*, which was not affected by hormone treatment (data not shown). Bars represent the mean ± SEM, and means with the same letter are not significantly different (ANOVA, Tukey's multiple comparison test; $P < .05$). Dashed lines indicate the calculated additive effect of combined hormone treatment.

5.812, $P < .05$) (Figure 6C). We also found that the frog KSM is transcribed, and combined hormone treatment caused a synergistic increase in *Klf9* eRNA in XTC-2 cells (Supplemental Figure 12).

Chromosomal looping brings the KSM into contact with the core promoter

Genome-wide investigation of long-range chromosomal interactions by ChIA-PET (55) for TR on tadpole tail fin epidermis (treated with 10nM T_3 for 24 h) showed an interaction between the frog KSM and the core promoter (and several other upstream genomic regions) (Figure 7A and Supplemental Materials and Methods). Similar chromosomal interaction is seen at the human KSM (data from the ENCODE project) (Supplemental Figure 13). 3C-qPCR assay (Supplemental Materials and Methods) conducted on chromatin isolated from HT-22 cells treated without or with T_3 plus CORT demonstrated interactions between the mouse *Klf9* core promoter and genomic regions that span the KSM (−4.9 kb from the TSS) (Figure 7B), which were not influenced by hormone treatment (data not shown). We detected no amplicons when the same primer-probe pairs were used with *Hin*dIII-digested and religated samples (negative ligation controls; data not shown).

Both the frog and human ChIA-PET datasets also identified far upstream regions with which the KSM interacts (Figure 7A and Supplemental Figure 13). In the frog this region is located at −39.2 kb from the TSS, in human at −72 kb and in mouse at −90 kb. There is clear conservation across several primates that had sequences available for this far upstream interacting region, and there are homologous regions in some other eutherian mammals (Supplemental Table 6). The frog and mammalian upstream interacting regions do not appear to be conserved. In human the −72-kb region has a strong peak for H3 lysine 4 (K4) monomethylation (Supplemental Figure 13), a mark of active enhancers (56).

Knockdown of *Med1* in HT-22 cells reduced hormone induction of *Klf9* mRNA and eRNAs

The Mediator complex subunit MED1 is important for linking enhancers to gene promoters by chromosomal looping (57–59) and associates with TR (60) and GR (61, 62) in a ligand-dependent manner. Subunits of the Mediator complex MED1 and MED12 exhibit distinct peaks that are associated with peaks of pol II at the mouse KSM and promoter, and at 4 upstream regions (Supplemental Figure 14 and Supplemental Table 6) (57). Transduction of HT-22 cells with *Med1* (Supplemental Materials and Methods) caused an approximately 60% reduction in *Med1* mRNA levels compared with the scrambled shRNA control (Supplemental Figure 15). Knockdown of *Med1* did not alter baseline *Klf9* mRNA but caused small but statistically significant reductions in the responses to T_3 and T_3 plus CORT. Baseline *Klf9* eRNA levels were similarly unaffected by *Med1* shRNA, but hormone re-

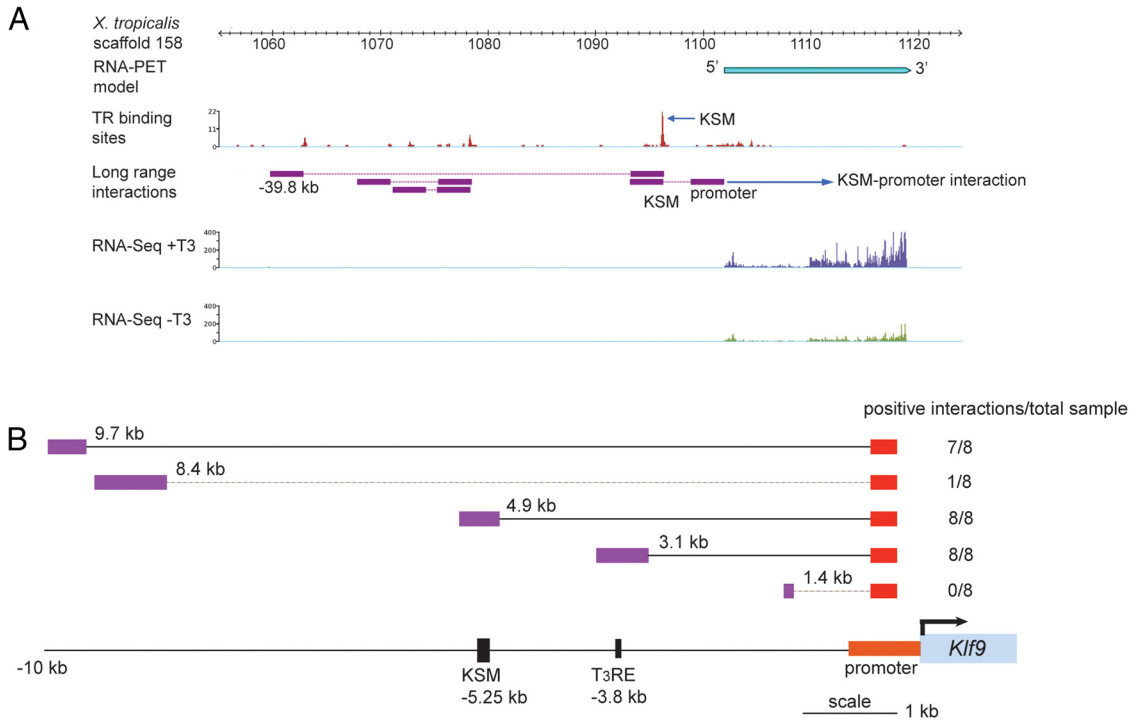

Figure 7. Chromosome looping brings the KSM into contact with the *Klf9* promoter. A, ChIA-PET shows that the frog KSM interacts with the *Klf9* promoter and a far upstream region (located at −39.8 kb upstream of the *Klf9* TSS). Chromatin from *X. tropicalis* tadpole tail fin epidermis (after a 24-h treatment with 10nM T_3 in vivo) was processed for TR ChIP, then ChIA-PET was conducted. Data for RNA-PET sequencing (103) and RNA sequencing (RNA-seq) (separate experiments conducted on tadpole tail fin harvested from tadpoles treated without or with 10nM T_3 for 24 h) at the frog *Klf9* locus are shown to identify the *Klf9* transcribed region and the TSS. The TR binding sites and the corresponding levels of TR bound across the *Klf9* locus, indicated as red peaks, were identified by the TR ChIP-seq component of the ChIA-PET dataset. Within the genomic region shown, the highest level of TR binding was seen at a region corresponding to the KSM (arrow). Long-range chromosomal interactions across the frog *Klf9* locus were identified by ChIA-PET and are indicated by the purple boxes connected by red lines. Note the interaction between the KSM and promoter, and the KSM and a far upstream region. B, 3C-qPCR analysis conducted on chromatin isolated from mouse HT-22 cells treated with vehicle or T_3 (30nM) plus CORT (100nM) for 4 hours. Primer sets that covered 5 locations upstream of the mouse *Klf9* locus were used, shown as distances in kilobases between the anchoring point within the promoter and the upstream region analyzed. The genomic locations of the KSM and the −3.8-kb T_3RE relative to the TSS are shown in the schematic at the bottom. The number of positive interactions detected for each genomic location is given in the column to the right; that is, the number of samples that showed qPCR amplification using the constant reverse primer and TaqMan probe, and the different forward primers (n = 8; 4 vehicle and 4 hormone-treated samples; there was no effect of hormone treatment on the interaction) (Supplemental Materials and Methods and Supplemental Table 3). Solid lines indicate significant interactions, dashed lines no significant interactions.

sponses were significantly reduced (Supplemental Figure 15). The relatively small reductions in the T_3-induced *Klf9* mRNA levels may be due to the incomplete knockdown of *Med1*.

Discussion

Cooperativity among TFs provides a means for cells to integrate multiple inputs to regulate gene transcription (12, 63, 64). Synergistic transcriptional responses, in part due to TF cooperativity, allow for 2 or more simultaneous signals to generate a response greater than additive, or for one signal to increase the sensitivity of the cell to a second, perhaps temporally delayed signal. Here, we report synergistic regulation of the *Klf9* gene by T_3 and CORT that may be explained by the presence of an evolutionarily conserved NR enhancer module located in the 5′-flanking region of the gene. This element (the KSM) contains a T_3RE that overlaps with a NFκB site and a GRE/MRE in close proximity. We show that liganded TR modulates recruitment of liganded GR and S5P pol II to the locus, and together, liganded TR and GR generate a synergistic transcriptional response. The region of the KSM is transcribed to generate eRNAs which are also synergistically induced by hormone action, and the production of eRNAs may depend on the loading of pol II from the promoter onto the KSM, or vice versa, requiring chromosomal looping between these genomic regions, mediated in part by the Mediator complex (57, 59, 65, 66).

An ultraconserved genomic region supports hormone synergy on *Klf9* gene transcription

Earlier findings from our group and others showed that *Xenopus* and mouse *Klf9* genes are regulated by T_3

and CORT (15–18). Gil-Ibanez et al (13) recently reported that treatment of primary cultures of cerebrocortical cells from wild-type mice with T_3 plus dexamethasone caused a synergistic increase in *Klf9* mRNA (see also Ref. 67). Here, we show that frog and mouse *Klf9* genes are synergistically induced by combined hormone treatment, further supporting that hormone regulation of this gene arose early in the evolution of tetrapods and has been conserved. An enhancer-reporter scan of the 5′-flanking region of the frog *Klf9* gene, and comparative genome sequence analysis revealed an ultraconserved (68, 69) approximately 180-bp sequence located 4–6 kb upstream of tetrapod *Klf9* genes that supports hormone synergy. It is located between the *Klf9* and *TRPM3* genes in tetrapod genomes. We could not find orthologous regions in other chordates, supporting that the KSM evolved in tetrapods. The KSM exhibits higher sequence conservation than the core promoter of *Klf9* genes, suggesting that it has been "ultraselected" (70).

Located within the KSM are 5 predicted hexanucleotide HSs (HS1–HS5) that are completely conserved across tetrapods and could therefore mediate NR actions. Our previous work showed that the GRE/MRE at −5.3 kb (HS1 and HS2) in the mouse KSM is a bona fide GRE/MRE (18). The HS4 and HS5 were previously identified by Furlow and Kanamori (23) in *Xenopus* and predicted to function as a DR+4 T_3RE in vivo. We confirmed that TR associates in chromatin with the orthologous mouse T_3RE at −5.23 kb, and mutational analysis showed that it is required for T_3-dependent transactivation. Although mutation of the GRE/MRE in the KSM reduced CORT and T_3 responses, mutation of the KSM T_3RE eliminated all hormone responses. Together with the observation that expression of a dnTR reduced the CORT response in tissue culture cells, our findings support that the T_3RE within the KSM plays a key role in modulating activity of this enhancer, and supports a model whereby liganded TR facilitates entry of GR to the KSM, thus supporting hormone synergy.

Within the KSM there are 2 predicted NFκB sites, one of which overlaps with the 5′ HS of the T_3RE. NFκB is comprised of a family of constitutively expressed TFs that are activated by the proinflammatory cytokine TNFα, among other signals, and bind to NFκB response elements of target genes as dimers (p50 and p65 dimers) (71). We found that p50 associates at the KSM and that activation of NFκB signaling by treatment of HT-22 cells with LPS acted synergistically with T_3 to induce *Klf9* mRNA. Thus, our findings support that TR-RXR and NFκB, possibly acting via a composite response element, cooperate to regulate transcription of *Klf9*. There are a few reports in the literature of interactions, both positive and negative, between the thyroid axis and inflammatory pathways mediated by NFκB (72–75), but this area requires more investigation.

Analysis of human ENCODE data support that the KSM is in a transcriptionally active chromatin environment that can be modulated by hormones. We found that histone modifications at the mouse KSM are modulated by hormone action. For example, T_3 or CORT increased acH3 and acH4, marks of transcriptionally active chromatin (76), and reduced H3 at the KSM, indicative of nucleosome repositioning and chromatin disassembly (77). The responses to combined hormone treatment were similar to the individual hormones, suggesting that although hormone responses are promoted by chromatin decompaction, hormone synergy is not dependent on further enhancement of histone acetylation or nucleosome repositioning (Supplemental Figure 10).

Enhancer transcription and chromatin interactions

We found that pol II is enriched at the KSM, which supports recent findings that the preinitiation complex is recruited to enhancers, and that pol II-bound enhancers may function in promoter targeting and regulation (78). Genome-wide analyses show that a large proportion of pol II, general TF, and chromatin modifying enzyme peaks are found at enhancers (56, 79–83), which is likely to be an important step in gene regulation that maintains the locus in a poised state without the risk of premature gene transcription (78, 84). In our studies, when both TR and GR were liganded, we saw enhanced recruitment of the elongating isoform (S5P) of pol II, which likely supported increased transcription, as evidenced by increased *Klf9* hnRNA, mRNA, and also eRNA.

Consistent with the enrichment of pol II at enhancer regions, recent findings show that enhancers are transcribed to give rise to a type of long, intergenic noncoding RNA (eRNA) (81). We detected eRNA transcripts from the region of the mouse and frog KSMs, and several expressed sequence tags associated with the KSM can be found in vertebrate genome databases. The synergistic response to combined hormone treatment was significantly greater for the *Klf9* eRNA than for the mRNA. Others have found that eRNAs increase in parallel to the associated protein coding genes in response to stimuli (79, 81). Genome-wide expression analysis of lncRNAs in mouse found that brain lncRNAs are more evolutionary constrained than lncRNAs expressed in other tissues, and tend to be close to genes that code for proteins involved with transcriptional regulation and nervous system development (85). Consistent with these findings, the KSM is highly conserved among tetrapods, *Klf9* exhibits strong developmental expression in the central nervous system

that depends on TH (16, 17, 22, 24), and KLF9 functions in T_3-dependent actions on neuron and oligodendrocyte differentiation (16, 27, 28, 31). We do not know whether the *Klf9* eRNA has a biological function, but we speculate that it could participate in communication between the KSM and the *Klf9* promoter. Recent findings support that lncRNAs may play a role in regulating gene transcription (78), possibly by influencing chromosomal looping through direct interaction with the Mediator complex, and thereby stabilizing the interaction between enhancer and promoter (59, 85–87).

Using ChIA-PET and 3C-qPCR analysis we found that chromosomal looping brings the KSM into contact with the *Klf9* core promoter (and several far upstream regions). Taken together with our functional analyses, these findings support that the KSM is a bona fide enhancer that communicates with the *Klf9* promoter to control gene transcription. The Mediator complex subunit MED1 functions in chromosomal looping (57–62) and ChIP sequencing data for MED1 and MED12 conducted on mouse embryonic stem cells (57) showed that both exhibited strong peaks at the KSM, *Klf9* promoter, and several upstream regions. Knockdown of MED1 in HT-22 cells reduced T_3-induction of *Klf9* mRNA and eRNAs. It is interesting that the eRNA was affected, even more strongly than the mRNA. This suggests that MED1 is important for enhancer transcription, perhaps for loading pol II from the promoter onto the enhancer. This would be consistent with the findings of Kim et al (81), who showed that eRNA synthesis depended on the presence of the promoter of the associated gene.

Molecular basis for hormone synergy

There are several proposed molecular mechanisms that could account for transcriptional synergy. For example, there may be enhanced recruitment of chromatin modifying enzymes to the locus (88); recruitment of an accessory TF at regulatory regions that only occurs in the presence of the synergizing NRs/TFs (89, 90); unidirectional or reciprocal cooperative binding of the synergizing NRs/TFs that may be attributed to enhanced decompaction of chromatin, thereby allowing for greater DNA-protein contact (91–96); and interaction between 2 regulatory regions mediated by protein-protein interactions and perhaps chromosomal looping (97, 98). It is likely that several of these mechanisms operate at the *Klf9* locus to support hormone synergy.

Our findings support that TRs, which are resident in chromatin in the unliganded state, modulate access of liganded GR to the KSM. We found that T_3 was required for CORT-induced recruitment of GR to the KSM, which also resulted in enhanced S5P pol II signal and strongly increased enhancer transcription. Forced expression of a dnTR unable to bind hormone and recruit coactivators suppressed CORT-mediated *Klf9* transactivation, suggesting that GR entry is dependent on chromatin state as modulated by the TR. Our findings also support that chromosomal looping is important for hormone action at the *Klf9* locus. Thus, TRs resident in chromatin in the unliganded state may function as "gate keepers" to modulate local chromatin structure (99), and therefore the accessibility of genomic loci to allow for developmental stage and physiological state-appropriate gene expression (100).

Acknowledgments

We thank Dr J. David Furlow (University of California, Davis, CA) for providing sequence data for the 2 *Xenopus laevis Klf9* genes, to Dr David Schubert (Salk Institute, La Jolla, CA) for providing the HT-22 cells, and Yun-Bo Shi (National Institute of Child Health and Development, National Institutes of Health, Bethesda, MD) for providing plasmids and antiserum. Elysha Cloyd and Daniel Brown provided technical assistance. Dr Kenneth Cadigan, Dr Audrey Seaholtz, and Dr Cunming Duan provided valuable comments on the project while serving on P.B.'s PhD dissertation committee. We also thank Patrice Bilesimo for the production of the TR ChIP material used for ChIA-PET; Zhenshui Zhang, Huay Mei Poh, and Alexis Khng Jiaying for construction of DNA-PET, RNA-PET, and Chia-PET libraries; and the Genome Institute of Singapore GTB sequencing group personnel for Illumina sequencing.

Address all correspondence and requests for reprints to: Robert J. Denver, PhD, Department of Molecular, Cellular and Developmental Biology, The University of Michigan, 3065C Natural Science Building, Ann Arbor, MI 48109-1048. E-mail: rdenver@umich.edu.

This work was supported by the National Institute of Neurological Disorders and Stroke, the National Institutes of Health Grant 1 R01 NS046690, and the National Science Foundation Grant IOS 0922583 (to R.J.D.). P.B. was supported by a predoctoral fellowship from the Rackham Graduate School and an Edwin Edwards Scholarship from the Department of Molecular, Cellular and Developmental Biology, University of Michigan. J.R.K. was supported by an MCubed grant from the University of Michigan. L.S. and Y.R. were supported by "CRESCENDO," an Integrated Project from FP6 (Contract LSHM-CT-2005–018652) and a Merlion Project (Contract 5.01.10). This research used the Cell and Molecular Biology Core of the Michigan Diabetes Research and Training Center funded by NIHP60 DK20572 from the National Institute of Diabetes and Digestive Kidney Diseases and the Vector Core at the University of Michigan.

Disclosure Summary: The authors have nothing to disclose.

References

1. **Denver RJ.** Stress hormones mediate environment-genotype interactions during amphibian development. *Gen Comp Endocrinol*. 2009;164:20–31.
2. **Bonett RM, Hoopfer ED, Denver RJ.** Molecular mechanisms of corticosteroid synergy with thyroid hormone during tadpole metamorphosis. *Gen Comp Endocrinol*. 2010;168:209–219.
3. **Metzger RJ, Klein OD, Martin GR, Krasnow MA.** The branching programme of mouse lung development. *Nature*. 2008;453:745–750.
4. **Pei L, Leblanc M, Barish G, et al.** Thyroid hormone receptor repression is linked to type I pneumocyte-associated respiratory distress syndrome. *Nat Med*. 2011;17:1466–1472.
5. **Smith BT, Sabry K.** Glucocorticoid-thyroid synergism in lung maturation: a mechanism involving epithelial-mesenchymal interaction. *Proc Natl Acad Sci USA*. 1983;80:1951–1954.
6. **McDonald MC, Henning SJ.** Synergistic effects of thyroxine and dexamethasone on enzyme ontogeny in rat small intestine. *Pediatr Res*. 1992;32:306–311.
7. **Amiel-Tison C, Cabrol D, Denver R, Jarreau PH, Papiernik E, Piazza PV.** Fetal adaptation to stress. Part I: acceleration of fetal maturation and earlier birth triggered by placental insufficiency in humans. *Early Hum Dev*. 2004;78:15–27.
8. **Challis JR, Sloboda D, Matthews SG, et al.** The fetal placental hypothalamic-pituitary-adrenal (HPA) axis, parturition and post natal health. *Mol Cell Endocrinol*. 2001;185:135–144.
9. **Porterfield SP, Hendrich CE.** The role of thyroid hormones in prenatal and neonatal neurological development–current perspectives. *Endocr Rev*. 1993;14:94–106.
10. **Welberg LA, Seckl JR.** Prenatal stress, glucocorticoids and the programming of the brain. *J Neuroendocrinol*. 2001;13:113–128.
11. **Ing H, O'Malley BW.** *The Steroid Hormone Receptor Superfamily: Molecular Mechanisms of Action*. New York, NY: Raven Press, Ltd; 1995.
12. **Courey AJ.** Cooperativity in transcriptional control. *Curr Biol*. 2001;11:R250–R252.
13. **Gil-Ibanez P, Bernal J, Morte B.** Thyroid hormone regulation of gene expression in primary cerebrocortical cells: role of thyroid hormone receptor subtypes and interactions with retinoic acid and glucocorticoids. *PLoS One*. 2014;9:e91692.
14. **Bagamasbad P, Denver RJ.** Thyroid hormone and glucocorticoids synergistically activate transcription of the basic transcription element binding protein 1 gene. Proceedings of the Endocrine Society Annual Meeting, San Francisco, CA, 2008.
15. **Bonett RM, Hu F, Bagamasbad P, Denver RJ.** Stressor and glucocorticoid-dependent induction of the immediate early gene kruppel-like factor 9: implications for neural development and plasticity. *Endocrinology*. 2009;150:1757–1765.
16. **Denver RJ, Ouellet L, Furling D, Kobayashi A, Fujii-Kuriyama Y, Puymirat J.** Basic transcription element-binding protein (BTEB) is a thyroid hormone-regulated gene in the developing central nervous system. Evidence for a role in neurite outgrowth. *J Biol Chem*. 1999;274:23128–23134.
17. **Denver RJ, Williamson KE.** Identification of a thyroid hormone response element in the mouse Kruppel-like factor 9 gene to explain its postnatal expression in the brain. *Endocrinology*. 2009;150:3935–3943.
18. **Bagamasbad P, Ziera T, Borden SA, et al.** Molecular basis for glucocorticoid induction of the Kruppel-like factor 9 gene in hippocampal neurons. *Endocrinology*. 2012;153:5334–5345.
19. **Chatonnet F, Guyot R, Benoît G, Flamant F.** Genome-wide analysis of thyroid hormone receptors shared and specific functions in neural cells. *Proc Natl Acad Sci USA*. 2013;110:E766–E775.
20. **Datson NA, Polman JA, de Jonge RT, et al.** Specific regulatory motifs predict glucocorticoid responsiveness of hippocampal gene expression. *Endocrinology*. 2011;152:3749–3757.
21. **Spörl F, Korge S, Jürchott K, et al.** Krüppel-like factor 9 is a circadian transcription factor in human epidermis that controls proliferation of keratinocytes. *Proc Natl Acad Sci USA*. 2012;109:10903–10908.
22. **Denver RJ, Pavgi S, Shi YB.** Thyroid hormone-dependent gene expression program for *Xenopus* neural development. *J Biol Chem*. 1997;272:8179–8188.
23. **Furlow JD, Kanamori A.** The transcription factor basic transcription element-binding protein 1 is a direct thyroid hormone response gene in the frog *Xenopus laevis*. *Endocrinology*. 2002;143:3295–3305.
24. **Hoopfer ED, Huang LY, Denver RJ.** Basic transcription element binding protein is a thyroid hormone-regulated transcription factor expressed during metamorphosis in *Xenopus laevis*. *Dev Growth Diff*. 2002;44:365–381.
25. **Knoedler JR, Denver RJ.** Krüppel-like factors are effectors of nuclear receptor signaling. *Gen Comp Endocrinol*. 2014;203:49–59.
26. **Avci HX, Lebrun C, Wehrlé R, et al.** Thyroid hormone triggers the developmental loss of axonal regenerative capacity via thyroid hormone receptor α1 and krüppel-like factor 9 in Purkinje cells. *Proc Natl Acad Sci USA*. 2012;109:14206–14211.
27. **Cayrou C, Denver RJ, Puymirat J.** Suppression of the basic transcription element-binding protein in brain neuronal cultures inhibits thyroid hormone-induced neurite branching. *Endocrinology*. 2002;143:2242–2249.
28. **Dugas JC, Ibrahim A, Barres BA.** The T3-induced gene KLF9 regulates oligodendrocyte differentiation and myelin regeneration. *Mol Cell Neurosci*. 2012;50:45–57.
29. **Lebrun C, Avci HX, Wehrlé R, et al.** Klf9 is necessary and sufficient for Purkinje cell survival in organotypic culture. *Mol Cell Neurosci*. 2013;54:9–21.
30. **Moore DL, Blackmore MG, Hu Y, et al.** KLF family members regulate intrinsic axon regeneration ability. *Science*. 2009;326:298–301.
31. **Morita M, Kobayashi A, Yamashita T, et al.** Functional analysis of basic transcription element binding protein by gene targeting technology. *Mol Cell Biol*. 2003;23:2489–2500.
32. **Scobie KN, Hall BJ, Wilke SA, et al.** Krüppel-like factor 9 is necessary for late-phase neuronal maturation in the developing dentate gyrus and during adult hippocampal neurogenesis. *J Neurosci*. 2009;29:9875–9887.
33. **Nieuwkoop PD, Faber J.** *Normal Table of Xenopus laevis (Daudin)*. New York, NY: Garland Publishing, Inc; 1994.
34. **Manzon RG, Denver RJ.** Regulation of pituitary thyrotropin gene expression during *Xenopus* metamorphosis: negative feedback is functional throughout metamorphosis. *J Endocrinol*. 2004;182:273–285.
35. **Samuels HH, Stanley F, Casanova J.** Depletion of L-3,5,3′-triiodothyronine and L-thyroxine in euthyroid calf serum for use in cell culture studies of the action of thyroid hormone. *Endocrinology*. 1979;105:80–85.
36. **Yao M, Schulkin J, Denver RJ.** Evolutionarily conserved glucocorticoid regulation of corticotropin-releasing factor expression. *Endocrinology*. 2008;149:2352–2360.
37. **Morimoto BH, Koshland DE Jr.** Induction and expression of long- and short-term neurosecretory potentiation in a neural cell line. *Neuron*. 1990;5:875–880.
38. **Morimoto BH, Koshland DE Jr.** Excitatory amino acid uptake and N-methyl-D-aspartate-mediated secretion in a neural cell line. *Proc Natl Acad Sci USA*. 1990;87:3518–3521.
39. **Maher P, Davis JB.** The role of monoamine metabolism in oxidative glutamate toxicity. *J Neurosci*. 1996;16:6394–6401.
40. **Sagara Y, Dargusch R, Chambers D, Davis J, Schubert D, Maher P.** Cellular mechanisms of resistance to chronic oxidative stress. *Free Radic Biol Med*. 1998;24:1375–1389.
41. **Sachs LM, Shi YB.** Targeted chromatin binding and histone acety-

lation in vivo by thyroid hormone receptor during amphibian development. *Proc Natl Acad Sci USA*. 2000;97:13138–13143.
42. **Sachs LM, Jones PL, Havis E, Rouse N, Demeneix BA, Shi YB.** Nuclear receptor corepressor recruitment by unliganded thyroid hormone receptor in gene repression during *Xenopus laevis* development. *Mol Cell Biol*. 2002;22:8527–8538.
43. **Buchholz DR, Paul BD, Shi YB.** Gene-specific changes in promoter occupancy by thyroid hormone receptor during frog metamorphosis. Implications for developmental gene regulation. *J Biol Chem*. 2005;280:41222–41228.
44. **Decherf S, Seugnet I, Kouidhi S, Lopez-Juarez A, Clerget-Froidevaux MS, Demeneix BA.** Thyroid hormone exerts negative feedback on hypothalamic type 4 melanocortin receptor expression. *Proc Natl Acad Sci USA*. 2010;107:4471–4476.
45. **Fullwood MJ, Ruan Y.** ChIP-based methods for the identification of long-range chromatin interactions. *J Cell Biochem*. 2009;107:30–39.
46. **Goh Y, Fullwood MJ, Poh HM, et al.** Chromatin interaction analysis with paired-end tag sequencing (ChIA-PET) for mapping chromatin interactions and understanding transcription regulation. *J Vis Exp*. 2012;(62).pii:3770.
47. **Bilesimo P, Jolivet P, Alfama G, et al.** Specific histone lysine 4 methylation patterns define TR-binding capacity and differentiate direct T3 responses. *Mol Endocrinol*. 2011;25:225–237.
48. **Fullwood MJ, Liu MH, Pan YF, et al.** An oestrogen-receptor-α-bound human chromatin interactome. *Nature*. 2009;462:58–64.
49. **Fullwood MJ, Wei CL, Liu ET, Ruan Y.** Next-generation DNA sequencing of paired-end tags (PET) for transcriptome and genome analyses. *Genome Res*. 2009;19:521–532.
50. **Hagège H, Klous P, Braem C, et al.** Quantitative analysis of chromosome conformation capture assays (3C-qPCR). *Nat Protoc*. 2007;2:1722–1733.
51. **Furlow JD, Brown DD.** In vitro and in vivo analysis of the regulation of a transcription factor gene by thyroid hormone during *Xenopus laevis* metamorphosis. *Mol Endocrinol*. 1999;13:2076–2089.
52. **Phatnani HP, Greenleaf AL.** Phosphorylation and functions of the RNA polymerase II CTD. *Genes Dev*. 2006;20:2922–2936.
53. **Shandilya J, Roberts SG.** The transcription cycle in eukaryotes: from productive initiation to RNA polymerase II recycling. *Biochim Biophys Acta*. 2012;1819:391–400.
54. **ENSEMBLE.** lincRNA at human Klf9 KSM. Ensembl release 79, March 2015. Accession No. MGI:1915498. Available at http://useast.ensembl.org/Mus_musculus/Gene/Summary?g=ENSMUSG00000044387;r=19:23134900-23135717;t=ENSMUST00000142712.
55. **Li G, Fullwood MJ, Xu H, et al.** ChIA-PET tool for comprehensive chromatin interaction analysis with paired-end tag sequencing. *Genome Biol*. 2010;11:R22.
56. **Heintzman ND, Hon GC, Hawkins RD, et al.** Histone modifications at human enhancers reflect global cell-type-specific gene expression. *Nature*. 2009;459:108–112.
57. **Kagey MH, Newman JJ, Bilodeau S, et al.** Mediator and cohesin connect gene expression and chromatin architecture. *Nature*. 2010;467:430–435.
58. **Park SW, Li G, Lin YP, et al.** Thyroid hormone-induced juxtaposition of regulatory elements/factors and chromatin remodeling of Crabp1 dependent on MED1/TRAP220. *Mol Cell*. 2005;19:643–653.
59. **Lai F, Orom UA, Cesaroni M, et al.** Activating RNAs associate with mediator to enhance chromatin architecture and transcription. *Nature*. 2013;494:497–501.
60. **Ito M, Roeder RG.** The TRAP/SMCC/mediator complex and thyroid hormone receptor function. *Trends Endocrinol Metab*. 2001;12:127–134.
61. **Chen W, Roeder RG.** The mediator subunit MED1/TRAP220 is required for optimal glucocorticoid receptor-mediated transcription activation. *Nucleic Acids Res*. 2007;35:6161–6169.
62. **Hittelman AB, Burakov D, Iñiguez-Lluhi JA, Freedman LP, Garabedian MJ.** Differential regulation of glucocorticoid receptor transcriptional activation via AF-1-associated proteins. *EMBO J*. 1999;18:5380–5388.
63. **Carey M.** The enhanceosome and transcriptional synergy. *Cell*. 1998;92:5–8.
64. **Herschlag D, Johnson FB.** Synergism in transcriptional activation: a kinetic view. *Genes Dev*. 1993;7:173–179.
65. **Malik S, Roeder RG.** The metazoan mediator co-activator complex as an integrative hub for transcriptional regulation. *Nat Rev Genet*. 2010;11:761–772.
66. **Whyte WA, Orlando DA, Hnisz D, et al.** Master transcription factors and mediator establish super-enhancers at key cell identity genes. *Cell*. 2013;153:307–319.
67. **Kulkarni SS, Buchholz D.** Beyond synergy: corticosterone and thyroid hormone have numerous interaction effects on gene regulation in *Xenopus tropicalis* tadpoles. *Endocrinology*. 2012;153:5309–5324.
68. **Bejerano G, Pheasant M, Makunin I, et al.** Ultraconserved elements in the human genome. *Science*. 2004;304:1321–1325.
69. **Faircloth BC, McCormack JE, Harvey MG, et al.** Ultra Conserved Elements. Available at http://ultraconserved.org/.
70. **Katzman S, Kern AD, Bejerano G, et al.** Human genome ultraconserved elements are ultraselected. *Science*. 2007;317:915–915.
71. **Vallabhapurapu S, Karin M.** Regulation and function of NF-κB transcription factors in the immune system. *Annu Rev Immunol*. 2009;27:693–733.
72. **Contreras-Jurado C, García-Serrano L, Gómez-Ferrería M, Costa C, Paramio JM, Aranda A.** The thyroid hormone receptors as modulators of skin proliferation and inflammation. *J Biol Chem*. 2011;286:24079–24088.
73. **Lasa M, Gil-Araujo B, Palafox M, Aranda A.** Thyroid hormone antagonizes tumor necrosis factor-α signaling in pituitary cells through the induction of dual specificity phosphatase 1. *Mol Endocrinol*. 2010;24:412–422.
74. **Huffman LJ, Prugh DJ, Brumbaugh K, Ding M.** Influence of hyperthyroidism on rat lung cytokine production and nuclear factor-κ B activation following ozone exposure. *Inhal Toxicol*. 2002;14:1161–1174.
75. **Nandakumar DN, Koner BC, Vinayagamoorthi R, et al.** Activation of NF-κ B in lymphocytes and increase in serum immunoglobulin in hyperthyroidism: possible role of oxidative stress. *Immunobiology*. 2008;213:409–415.
76. **Aoyagi S, Archer TK.** Dynamics of coactivator recruitment and chromatin modifications during nuclear receptor mediated transcription. *Mol Cell Endocrinol*. 2008;280:1–5.
77. **Luebben WR, Sharma N, Nyborg JK.** Nucleosome eviction and activated transcription require p300 acetylation of histone H3 lysine 14. *Proc Natl Acad Sci USA*. 2010;107:19254–19259.
78. **Natoli G, Andrau JC.** Noncoding transcription at enhancers: general principles and functional models. *Annu Rev Genet*. 2012;46:1–19.
79. **De Santa F, Barozzi I, Mietton F, et al.** A large fraction of extragenic RNA Pol II transcription sites overlap enhancers. *PLoS Biol*. 2010;8:e1000384.
80. **Heintzman ND, Stuart RK, Hon G, et al.** Distinct and predictive chromatin signatures of transcriptional promoters and enhancers in the human genome. *Nat Genet*. 2007;39:311–318.
81. **Kim TK, Hemberg M, Gray JM, et al.** Widespread transcription at neuronal activity-regulated enhancers. *Nature*. 2010;465:182–187.
82. **Koch F, Fenouil R, Gut M, et al.** Transcription initiation platforms and GTF recruitment at tissue-specific enhancers and promoters. *Nat Struct Mol Biol*. 2011;18:956–963.
83. **Ørom UA, Shiekhattar R.** Long noncoding RNAs usher in a new era in the biology of enhancers. *Cell*. 2013;154:1190–1193.

84. **Szutorisz H, Dillon N, Tora L.** The role of enhancers as centres for general transcription factor recruitment. *Trends Biochem Sci*. 2005;30:593–599.
85. **Ponjavic J, Oliver PL, Lunter G, Ponting CP.** Genomic and transcriptional co-localization of protein-coding and long non-coding RNA pairs in the developing brain. *PLoS Genet*. 2009;5:e1000617.
86. **Ørom UA, Derrien T, Beringer M, et al.** Long noncoding RNAs with enhancer-like function in human cells. *Cell*. 2010;143:46–58.
87. **Li W, Notani D, Ma Q, et al.** Functional roles of enhancer RNAs for oestrogen-dependent transcriptional activation. *Nature*. 2013;498:516–520.
88. **Bagamasbad P, Denver RJ.** Mechanisms and significance of nuclear receptor auto- and cross-regulation. *Gen Comp Endocrinol*. 2011;170:3–17.
89. **Brüggemeier U, Rogge L, Winnacker EL, Beato M.** Nuclear factor I acts as a transcription factor on the MMTV promoter but competes with steroid hormone receptors for DNA binding. *EMBO J*. 1990;9:2233–2239.
90. **Wyszomierski SL, Rosen JM.** Cooperative effects of STAT5 (signal transducer and activator of transcription 5) and C/EBPβ (CCAAT/enhancer-binding protein-β) on β-casein gene transcription are mediated by the glucocorticoid receptor. *Mol Endocrinol*. 2001;15:228–240.
91. **Hebbar PB, Archer TK.** Chromatin-dependent cooperativity between site-specific transcription factors in vivo. *J Biol Chem*. 2007;282:8284–8291.
92. **Gummow BM, Scheys JO, Cancelli VR, Hammer GD.** Reciprocal regulation of a glucocorticoid receptor-steroidogenic factor-1 transcription complex on the Dax-1 promoter by glucocorticoids and adrenocorticotropic hormone in the adrenal cortex. *Mol Endocrinol*. 2006;20:2711–2723.
93. **Takeda T, Kurachi H, Yamamoto T, et al.** Crosstalk between the interleukin-6 (IL-6)-JAK-STAT and the glucocorticoid-nuclear receptor pathway: synergistic activation of IL-6 response element by IL-6 and glucocorticoid. *J Endocrinol*. 1998;159:323–330.
94. **Lerner L, Henriksen MA, Zhang X, Darnell JE Jr.** STAT3-dependent enhanceosome assembly and disassembly: synergy with GR for full transcriptional increase of the α 2-macroglobulin gene. *Genes Dev*. 2003;17:2564–2577.
95. **Latchoumanin O, Mynard V, Devin-Leclerc J, Dugué MA, Bertagna X, Catelli MG.** Reversal of glucocorticoids-dependent proopiomelanocortin gene inhibition by leukemia inhibitory factor. *Endocrinology*. 2007;148:422–432.
96. **Tan SH, Dagvadorj A, Shen F, et al.** Transcription factor Stat5 synergizes with androgen receptor in prostate cancer cells. *Cancer Res*. 2008;68:236–248.
97. **Kabotyanski EB, Huetter M, Xian W, Rijnkels M, Rosen JM.** Integration of prolactin and glucocorticoid signaling at the β-casein promoter and enhancer by ordered recruitment of specific transcription factors and chromatin modifiers. *Mol Endocrinol*. 2006;20:2355–2368.
98. **Ong CT, Corces VG.** Enhancer function: new insights into the regulation of tissue-specific gene expression. *Nat Rev Genet*. 2011;12:283–293.
99. **Cheng SY, Leonard JL, Davis PJ.** Molecular aspects of thyroid hormone actions. *Endocr Rev*. 2010;31:139–170.
100. **Shi YB.** Unliganded thyroid hormone receptor regulates metamorphic timing via the recruitment of histone deacetylase complexes. *Curr Top Dev Biol*. 2013;105:275–297.
101. **Ruan X, Ruan Y.** Genome wide full-length transcript analysis using 5′ and 3′ paired-end-tag next generation sequencing (RNA-PET). *Methods Mol Biol*. 2012;809:535–562.